

Improving Neural Additive Models with Bayesian Principles

Kouroche Bouchiat¹

Alexander Immer^{1,2}

Hugo Yèche¹

Gunnar Rätsch¹

Vincent Fortuin^{3,4}

¹ETH Zürich

²MPI-IS Tübingen

³Helmholtz AI

⁴TU Munich

Abstract

Neural additive models (NAMs) can improve the interpretability of deep neural networks by handling input features in separate additive sub-networks. However, they lack inherent mechanisms that provide calibrated uncertainties and enable selection of relevant features and interactions. Approaching NAMs from a Bayesian perspective, we enhance them in three primary ways, namely by a) providing credible intervals for the individual additive sub-networks; b) estimating the marginal likelihood to perform an implicit selection of features via an empirical Bayes procedure; and c) enabling a ranking of feature pairs as candidates for second-order interaction in fine-tuned models. In particular, we develop Laplace-approximated NAMs (LA-NAMs), which show improved empirical performance on tabular datasets and challenging real-world medical tasks.

1 Introduction

Over the past decade, deep neural networks (DNNs) have found successful applications in numerous fields, ranging from computer vision and speech recognition to natural language processing and recommendation systems. This success is often attributed to the growing availability of data in all areas of science and industry. However, the inherent complexity and lack of transparency of DNNs have impeded their use in domains where understanding the reasoning behind their decision-making process is crucial (Pumplun et al., 2021; Veale et al., 2018).

Model-agnostic methods, such as partial dependence

(Friedman, 2001), SHAP (Lundberg and Lee, 2017), and LIME (Ribeiro et al., 2016), provide a standardized approach to explaining predictions in machine learning, but the explanations they generate for DNNs are not faithful representations of their full complexity (Rudin, 2019). Instead, one can promote interpretability in DNNs by acting directly on their architecture and training procedure. For instance, in generalized additive models (Hastie and Tibshirani, 1999), the response variable y is associated with inputs x_1, \dots, x_p using an additive structure of the form

$$g(\mathbb{E}[y | x_1, \dots, x_p]) = \beta_0 + f_1(x_1) + \dots + f_p(x_p). \quad (1)$$

The neural additive models (NAMs) introduced by Agarwal et al. (2021) hinge on this concept. In this model architecture, each input dimension is processed by a distinct sub-network, elucidating the connections between the input features and the model’s predictions. However, restricting neural network models in this way can lead to overconfidence, overreliance on uninformative features and obliviousness to underlying feature interactions.

Main contributions. In this work, we (a) propose a Bayesian variant of the NAM by deriving a tailored *linearized Laplace inference* (MacKay, 1994) on the subnetworks. We show that this leads to improved interpretability via **increased smoothness and enhanced uncertainty estimation**. Moreover, (b) this model construction enables the estimation of the marginal likelihood, which serves as a Bayesian model selection criterion. This allows us to effectively **ignore uninformative features**, thus further enhancing robustness and trustworthiness. Also, (c) in situations where strong feature interactions exist in the ground-truth function and cause poor performance of first-order additive models, we leverage our Laplace approximation to **automatically select informative feature interactions**, which can then be added to the model to improve its overall performance. Finally, (d) we show on tabular regression and classifications benchmarks, as well as on challenging real-world medical tasks, that our proposed LA-NAM performs com-

Preprint. Under review.

Correspondance to: {kbouchiat@student.ethz.ch},
{alexander.immer@inf.ethz.ch}

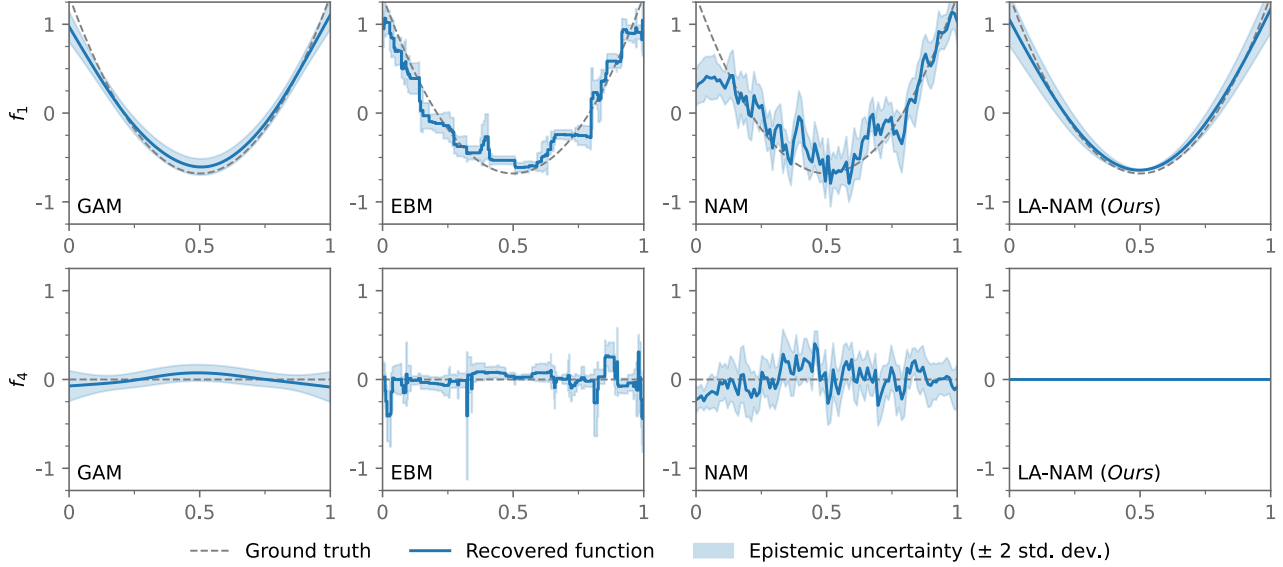


Figure 1: Regression on a synthetic dataset with known additive structure (see Section 4.1 and Appendix B.8 for details). While the baselines yield sub-optimal fits, the LA-NAM fits the data well, provides useful uncertainty estimates, and correctly ignores the uninformative feature (f_4 , bottom.)

petitively with the baselines while offering more interpretable global and local explanations.

2 Related Work

Neural additive models. Several constructions have been proposed for the generalized additive models (GAMs) of Hastie and Tibshirani (1999), using both smoothing splines (Wahba, 1983) and gradient-boosted decision trees (Friedman, 2001; Lou et al., 2012, 2013). Neural networks are also particularly compelling candidates for the construction of GAMs since they can be made to approximate continuous functions up to arbitrary precision given sufficient complexity (Cybenko, 1989; Maierov and Pinkus, 1999; Lu et al., 2017). The neural additive model (NAM) proposed by Agarwal et al. (2021) is constructed using ensembles of ExU feed-forward networks, in which weights are learned in logarithmic space in order to fit jagged functions. The GAMI-Net proposed around the same time by Yang et al. (2021) is closely related: Single networks are used instead of an ensemble, and the model also supports learning feature interaction terms. Recently proposed extensions to NAMs include feature selection through sparse regularization of the feature nets (Xu et al., 2022), generation of confidence intervals using regression spline basis expansion (Luber et al., 2023), and estimation of the skewness, heteroscedasticity, and kurtosis of the underlying data distributions (Thielmann et al., 2023). Our work further extends NAMs via Laplace-

approximated Bayesian inference to endow them with principled uncertainty estimation and feature interaction and selection abilities within a unified Bayesian framework.

Bayesian neural networks. Bayesian neural networks promise to marry the expressivity of neural networks with the principled statistical properties of Bayesian inference (MacKay, 1992; Neal, 1993). There are many approximate inference techniques, such as Laplace inference (Laplace, 1774; MacKay, 1992; Khan et al., 2019; Daxberger et al., 2021a), stochastic weight averaging (Izmailov et al., 2018; Maddox et al., 2019), dropout (Gal and Ghahramani, 2016; Kingma et al., 2015), variational inference (e.g., Graves, 2011; Blundell et al., 2015; Khan et al., 2018), ensemble-based methods (Lakshminarayanan et al., 2017; Wang et al., 2019; Ciosek et al., 2020; He et al., 2020; D’Angelo and Fortuin, 2021), and sampling approaches (e.g., Neal, 1993; Neal et al., 2011; Welling and Teh, 2011; Garriga-Alonso and Fortuin, 2021). In our work, we leverage linearized Laplace (MacKay, 1994; Khan et al., 2019; Foong et al., 2019; Immer et al., 2021b) for inference in Bayesian NAMs. This is motivated by the Laplace approximation’s ability to provide not only reliable predictive uncertainties but also marginal likelihood estimates (Immer et al., 2021a), the latter of which is not yet readily available with most other approximations.

Refer to Appendix C for a more detailed treatment of the related work.

3 Method

We introduce a Bayesian formulation of neural additive models and propose a tractable approximation which is based on linearized Laplace inference of neural networks (MacKay, 1991; Khan et al., 2019; Foong et al., 2019; Immer et al., 2021b). The proposed model (LA-NAM) relies on a block-diagonal variant of the Gauss-Newton approximation with Kronecker factorization (Martens and Grosse, 2015) and uses the associated predictive and log-marginal likelihood (Immer et al., 2021a,b) to estimate feature-wise uncertainty and perform feature and interaction selection.

3.1 Bayesian Neural Additive Model

We consider supervised learning tasks with inputs $\mathbf{x}_n \in \mathbb{R}^D$ and outputs y_n where $y_n \in \mathbb{R}$ in regression and $y_n \in \{0, 1\}$ in classification, and denote $\mathcal{D} = \{(\mathbf{x}_n, y_n)\}_{n=1}^N$ as the training set containing N sample pairs. A neural additive model is a neural network f consisting of sub-networks f_1, \dots, f_D with parameters $\boldsymbol{\theta} = \{\boldsymbol{\theta}_1, \dots, \boldsymbol{\theta}_D\}$, wherein each sub-network applies to an individual input dimension,

$$f(\mathbf{x}; \boldsymbol{\theta}) = f_1(x_1; \boldsymbol{\theta}_1) + \dots + f_D(x_D; \boldsymbol{\theta}_D). \quad (2)$$

We refer to the sub-networks $f_d : \mathbb{R} \times \mathbb{R}^P \rightarrow \mathbb{R}$, with parameters $\boldsymbol{\theta}_d \in \mathbb{R}^P$, as *feature networks*. For simplicity, we assume that all feature networks share the same architecture. In practice, it can vary to accommodate mixed feature types such as binary or categorical features. The sum is mapped to an output y using a likelihood function $p(\mathcal{D} | \boldsymbol{\theta}_1, \dots, \boldsymbol{\theta}_D)$ with inverse link function $g^{-1}(\cdot)$, e.g., the sigmoid for classification, such that we have $\mathbb{E}[y | \mathbf{x}] = g^{-1}(f(\mathbf{x}))$, and

$$p(\mathcal{D} | \boldsymbol{\theta}) = \prod_{n=1}^N p(y_n | f(\mathbf{x}_n; \boldsymbol{\theta})). \quad (3)$$

We impose a zero-mean Gaussian prior distribution over the parameters of each feature network with prior precision hyperparameters $\boldsymbol{\lambda} = \{\lambda_1, \dots, \lambda_D\}$,

$$p(\boldsymbol{\theta}) = p(\boldsymbol{\theta}_1, \dots, \boldsymbol{\theta}_D | \boldsymbol{\lambda}) = \prod_{d=1}^D \mathcal{N}(\boldsymbol{\theta}_d; \mathbf{0}, \lambda_d^{-1} \mathbf{I}). \quad (4)$$

These terms adaptively regularize the network parameters and enable feature selection in a similar fashion to automatic relevance determination (ARD; MacKay, 1994; Neal, 1995). Large values push the corresponding feature networks toward zero and low values encourage highly non-linear fits. In practice, one can also use separate priors and precision terms for each layer of each feature network, as this has been shown to be beneficial in linearized Laplace (Immer et al., 2021a; Antorán et al., 2022).

3.2 Laplace-Approximated NAM

We choose to rely on the linearized Laplace approximation (Laplace, 1774; MacKay, 1991; Khan et al., 2019) to estimate the posterior and log-marginal likelihood. This choice is motivated by the well-established posterior predictive (Foong et al., 2019; Immer et al., 2021b) which is known to provide calibrated estimates of uncertainty (Daxberger et al., 2021a). Additionally useful is the approximation’s ability to yield differentiable estimates of the log-marginal likelihood for on-line optimization of the observation noise and feature networks’ prior precisions (Immer et al., 2021a), something which is not easily feasible with other approximate inference methods as we discuss in Appendix B.1.

Similar to Immer et al. (2021b), we linearize the model around a parameter estimate $\boldsymbol{\theta}^* = \{\boldsymbol{\theta}_1^*, \dots, \boldsymbol{\theta}_D^*\}$,

$$f^{\text{lin}}(\mathbf{x}; \boldsymbol{\theta}^*) = f_1^{\text{lin}}(x_1; \boldsymbol{\theta}_1^*) + \dots + f_D^{\text{lin}}(x_D; \boldsymbol{\theta}_D^*), \quad (5)$$

$$f_d^{\text{lin}}(x_d; \boldsymbol{\theta}_d^*) = f_d(x_d; \boldsymbol{\theta}_d^*) + \mathcal{J}_{\boldsymbol{\theta}^*}^{(d)}(x_d)(\boldsymbol{\theta}_d - \boldsymbol{\theta}_d^*), \quad (6)$$

where $\mathcal{J}_{\boldsymbol{\theta}^*}^{(d)} : \mathbb{R} \rightarrow \mathbb{R}^P$ is the Jacobian of the d -th feature network w.r.t. $\boldsymbol{\theta}_d$, such that $[\mathcal{J}_{\boldsymbol{\theta}^*}^{(d)}]_i = \partial f_d / \partial \theta_{d,i}$. This step follows from the linearity of the gradient operator and the fact that $\partial f_d / \partial \theta_{d',i} = 0$ for $d \neq d'$.

This reduces the model to a generalized linear model in the Jacobians whose posterior can be approximated with a block-diagonal Laplace approximation as

$$q(\boldsymbol{\theta}) = \mathcal{N}(\boldsymbol{\theta}^*, \boldsymbol{\Sigma}^*), \quad \boldsymbol{\Sigma}^* \approx \begin{bmatrix} \boldsymbol{\Sigma}_1 & \dots & 0 \\ \vdots & \ddots & \vdots \\ 0 & \dots & \boldsymbol{\Sigma}_D \end{bmatrix}. \quad (7)$$

where the diagonal covariance blocks are determined using the feature network Jacobians and second derivatives of the log-likelihood, $\gamma_n = -\frac{\partial^2}{\partial f^2} \log p(y_n | f_n)$, by

$$\boldsymbol{\Sigma}_d = \left[\sum_{n=1}^N \gamma_n \cdot \mathcal{J}_{\boldsymbol{\theta}^*}^{(d)}(x_{n,d})^\top \mathcal{J}_{\boldsymbol{\theta}^*}^{(d)}(x_{n,d}) + \lambda_d \mathbf{I} \right]^{-1}. \quad (8)$$

The approximation also leads to an additive structure over feature networks in the log-marginal likelihood,

$$\log p(\mathcal{D} | \boldsymbol{\lambda}) \approx \log p(\mathcal{D}, \boldsymbol{\theta}^* | \boldsymbol{\lambda}) - \frac{1}{2} \log \left| \frac{1}{2\pi} \boldsymbol{\Sigma} \right| \quad (9)$$

$$\geq \log p(\mathcal{D}, \boldsymbol{\theta}^* | \boldsymbol{\lambda}) - \frac{1}{2} \sum_d \log \left| \frac{1}{2\pi} \boldsymbol{\Sigma}_d \right| \quad (10)$$

where the lower bound is a consequence of the block-diagonal structure (Immer et al., 2023, Thm. 1).

In practice, we further approximate the covariance blocks $\boldsymbol{\Sigma}_d$ by using layer-wise Kronecker factorization (Ritter et al., 2018; Daxberger et al., 2021a), thereby avoiding the memory and computational complexity associated with the quadratic size in the number of parameters P .

3.2.1 Feature Network Selection

During training, the feature networks are implicitly compared and selected using adaptive regularization. This selection mechanism arises from the optimization of the lower bound on the log-marginal likelihood in Eq. (10), which we denote here as $\log q(\mathcal{D} | \lambda)$. In the automatic relevance determination (ARD) procedure of MacKay (1994) and Neal (1995), parameters of the first layer are grouped together according to their input feature and regularized as one. In our case, one feature networks corresponds to one group.

We maximize the lower bound on the log-marginal likelihood, $\max_{\lambda} \log q(\mathcal{D} | \lambda)$, by taking gradient-based¹ updates during training as in Immer et al. (2021a):

$$\frac{\partial}{\partial \lambda_d} \log q(\mathcal{D} | \lambda) = \frac{P}{\lambda_d} - \|\theta_d^*\|_2^2 - \text{Tr } \Sigma_d. \quad (11)$$

An intuition of the corresponding closed-form update derived by MacKay (1991) is given in Tipping (2001): the optimal value of λ_d is a measure of the concentration of Σ_d relative to the prior and depends on how well the data determines the parameters θ_d . Large values of λ_d lead to strong regularization and effectively switch off the d -th feature network. This is depicted in Fig. 1, where our method demonstrates its ability to disregard an uninformative feature. As a result, the procedure can lead to enhanced model interpretability and robustness as it redirects the attention to smaller subsets of informative features.

3.2.2 Feature Network Predictive

Function-space inference of the feature networks is also made possible by the linearization of the model. Given an unobserved sample \mathbf{x}^* , the predictive variance of the linearized model $f^{\text{lin},*}$ corresponds to the sum of predictive variances of the linearized feature networks,

$$\mathbb{V}[f^{\text{lin},*} | \mathbf{x}^*] = \sum_d \mathbb{V}[f_d^{\text{lin},*} | x_d^*] \quad (12)$$

$$= \sum_d \mathcal{J}_{\theta^*}^{(d)}(x_d^*)^\top \Sigma_d \mathcal{J}_{\theta^*}^{(d)}(x_d^*). \quad (13)$$

This is a direct consequence of the block-diagonal structure in the approximation of Eq. (7), which we discuss in further detail in Appendix A.1.

As training progresses, the feature networks may shift to satisfy a global intercept value in their sum. They should therefore be shifted back around zero before visualization by removing the expected contribution,

$$\hat{f}_d(x_d^*) = f_d(x_d^*) - \mathbb{E}_{\mathbf{x} \sim p(\mathcal{D})}[f_d(x_d)]. \quad (14)$$

Importantly, this adjustment does not affect the predictive variance $\mathbb{V}[f_d^{\text{lin},*}]$. This variance estimate can

¹We also conducted experiments with closed-form updates of MacKay (1991) and obtained comparable results.

be used to generate credible intervals for local and global explanations of the model, as shown in Fig. 2 and Fig. 4. Notably, this allows the model to not only communicate on which data points it is uncertain, but also which features are responsible for the uncertainty.

3.2.3 Feature Network Interaction

Many datasets are not truly additive and thus require modeling interactions of features to adequately fit the data. However, it is *a priori* unclear which features exhibit underlying interactions. As the search space grows exponentially for higher-order interactions, we focus here on the second order. In second-order feature interaction detection, the goal is to find a subset of all existing D^2 interaction pairs that, when added to the model, maximize the gain in performance. For each selected interacting pair (d, d') , we can then append a *joint feature network* $f_{d,d'}(x_d, x_{d'})$ and perform fine-tuning of the model with the appended networks as part of a secondary training stage.

Our method for detecting and selecting second-order interactions makes use of the mutual information between feature networks. If the mutual information between the feature network parameters θ_d and $\theta_{d'}$ is high, then conditioning on the values of either of these should provide information about the other and thus, their functions. This can be an indication that a joint feature network for this pair may improve the data fit.

Although the mutual information between feature networks is zero in the approximation of Eq. (7), this is not necessarily the case in the true posterior. For the purpose of determining mutual information of the feature networks, we therefore fit a separate last-layer Laplace approximation of the model. After the first training stage, we consider only the scalar output multiplier weights θ_d of each feature network and for each candidate pair of features (d, d') determine the scalar marginal variances σ_d^2 , $\sigma_{d'}^2$, and $\sigma_{d,d'}^2$ in the resulting $D \times D$ posterior covariance matrix. The mutual information can then be approximated using

$$I(\theta_d; \theta_{d'}) = H(\theta_d) + H(\theta_{d'}) - H(\theta_d, \theta_{d'}) \quad (15)$$

$$\approx \frac{1}{2} \log [\sigma_d^2 \sigma_{d'}^2 (\sigma_d^2 \sigma_{d'}^2 - \sigma_{d,d'}^2)^{-1}] \quad (16)$$

$$= \frac{1}{2} \log [1 - \text{Corr}(\theta_d, \theta_{d'})^2]^{-1}. \quad (17)$$

Finally, we select interactions by computing the mutual information for all feature pairs and taking the top- k highest scoring pairs. Importantly, this can be done after training in the first stage and without the need for an additional model to assess interaction strength. We show in the experiments that with only a few second-order interactions selected this way the performance of the additive model can improve to be at the level of a fully-interacting baseline.

Table 1: Negative test log-likelihood (lower is better) on the UCI regression (top) and classification (bottom) benchmarks. Results within one standard error of the best performance among additive models are in bold. Results in green or red indicate an improvement or decrease beyond one standard error when compared to the corresponding model without second-order interactions. The LA-NAM performs competitively with the other additive models and often outperforms the NAM. Moreover, when 10 interactions are selected, it almost always improves and often reaches competitive performance with the fully-interacting LightGBM.

Dataset	EBM	NAM	LA-NAM	EBM ₁₀	LA-NAM ₁₀	LightGBM
autompg ($n = 392$)	2.64 \pm 0.10	2.69 \pm 0.16	2.46 \pm 0.08	2.99 \pm 0.29	2.45 \pm 0.09	2.53 \pm 0.07
concrete ($n = 1030$)	3.20 \pm 0.12	3.46 \pm 0.12	3.25 \pm 0.03	3.53 \pm 0.20	3.18 \pm 0.04	3.09 \pm 0.09
energy ($n = 768$)	1.46 \pm 0.02	1.48 \pm 0.02	1.44 \pm 0.02	0.67 \pm 0.05	1.11 \pm 0.12	0.81 \pm 0.05
kin8nm ($n = 8192$)	-0.20 \pm 0.01	-0.18 \pm 0.01	-0.20 \pm 0.00	-0.34 \pm 0.01	-0.28 \pm 0.02	-0.50 \pm 0.03
naval ($n = 11934$)	-3.15 \pm 0.00	-3.87 \pm 0.01	-7.24 \pm 0.01	-3.60 \pm 0.01	-7.44 \pm 0.07	-5.19 \pm 0.01
power ($n = 9568$)	2.79 \pm 0.02	2.89 \pm 0.02	2.85 \pm 0.01	2.72 \pm 0.02	2.79 \pm 0.01	2.67 \pm 0.02
protein ($n = 45730$)	3.00 \pm 0.00	3.02 \pm 0.00	3.02 \pm 0.00	2.89 \pm 0.01	2.94 \pm 0.01	2.83 \pm 0.00
wine ($n = 1599$)	0.99 \pm 0.03	1.02 \pm 0.04	0.98 \pm 0.03	1.01 \pm 0.04	0.97 \pm 0.03	0.96 \pm 0.03
yacht ($n = 308$)	1.93 \pm 0.13	2.24 \pm 0.08	1.81 \pm 0.10	4.80 \pm 1.59	0.76 \pm 0.20	1.37 \pm 0.28
australian ($n = 690$)	0.33 \pm 0.03	0.38 \pm 0.04	0.34 \pm 0.03	0.32 \pm 0.04	0.34 \pm 0.03	0.31 \pm 0.03
breast ($n = 569$)	0.12 \pm 0.02	0.16 \pm 0.03	0.10 \pm 0.02	0.12 \pm 0.02	0.10 \pm 0.02	0.09 \pm 0.01
heart ($n = 270$)	0.40 \pm 0.02	0.41 \pm 0.04	0.33 \pm 0.02	0.41 \pm 0.03	0.33 \pm 0.03	0.39 \pm 0.04
ionosphere ($n = 351$)	0.23 \pm 0.02	0.31 \pm 0.04	0.25 \pm 0.04	0.22 \pm 0.02	0.27 \pm 0.03	0.19 \pm 0.03
parkinsons ($n = 195$)	0.28 \pm 0.05	0.29 \pm 0.04	0.26 \pm 0.03	0.36 \pm 0.12	0.25 \pm 0.03	0.22 \pm 0.03

4 Experiments

We evaluate the proposed LA-NAM on a collection of synthetic and real-world datasets, and highlight its potential in assisting decision-making in the medical field. To assess performance, we compare against the original NAM of Agarwal et al. (2021) and various other generalized additive models, namely, the smoothing spline *generalized additive model* (GAM), with smoothing parameters selected via cross-validation (Hastie and Tibshirani, 1999; Servén et al., 2018), and the gradient boosting-based *explainable boosting model* (EBM) (Lou et al., 2012; Nori et al., 2019). We also benchmark against LightGBM (Ke et al., 2017), a state-of-the-art fully-interacting model which approximates the maximal attainable performance in tabular regression and classification tasks (Grinsztajn et al., 2022). Detailed information regarding the experimental setup is provided in Appendix B.7.

Both the NAM and EBM, which are included in our comparative analysis, lack a built-in notion of epistemic uncertainty. Figures that provide the uncertainty associated with the predictions made by the NAM use the standard deviation of the recovered functions across a deep ensemble of NAMS. For the EBM, bootstrapping is leveraged to estimate uncertainty.

4.1 Illustrative Example

To demonstrate the capability of recovering purely additive structures from noisy data, we constructed a synthetic regression dataset for which the true addi-

tive functions are known. Generalized additive models are expected to accurately recover the additive functions present in this dataset since it is designed in such a way that there is no interaction between the input features.

In Fig. 1, we show the recovered functions for f_1 and f_4 along with the ground-truth quadratic function f_1 and zero function f_4 . The NAM exhibits pronounced jumpy behavior due to the presence of noise, resulting in a considerably poor mean fit. In contrast, the proposed LA-NAM fits the data accurately while maintaining a good estimate of epistemic uncertainty. It is less susceptible to misattributing noise to the recovered functions compared to the other baselines. This is particularly striking for the uninformative function f_4 , since only the LA-NAM correctly predicts that it should have no effect. The details, along with a visualization of this experiment, are deferred to Appendix B.8.

4.2 UCI Regression and Classification

We now benchmark the LA-NAM and baselines on the standard selection of UCI regression and binary classification datasets. Each dataset is split into five cross-validation folds and the mean and standard error of model performance are reported across folds. We split off 12.5% of the training data as validation data for the NAM and EBM. This extra validation data is not required for the LA-NAM, since it is tuned using the estimated log-marginal likelihood. Additionally, both the LA-NAM and EBM have support for selecting and fitting second-order feature interactions, further en-

Table 2: Comparison of model performance on ICU mortality prediction tasks. Mean and standard error over five runs with different random seeds are reported. AUROC and AUPRC are given in percent. Bolded values indicate best performance within additive models; green highlights an improvement when second-order interactions are added. Again, the LA-NAM generally outperforms the NAM, and improves with 10 interacting features on MIMIC-III, becoming competitive with the fully-interacting LightGBM gold-standard.

Task	MIMIC-III ICU Mortality			HiRID ICU Mortality		
	AUROC (\uparrow)	AUPRC (\uparrow)	NLL (\downarrow)	AUROC (\uparrow)	AUPRC (\uparrow)	NLL (\downarrow)
EBM	78.7 \pm 0.02	33.6 \pm 0.04	0.268 \pm 9e-5	90.2 \pm 0.03	59.2 \pm 0.10	0.177 \pm 2e-4
NAM	77.6 \pm 0.03	32.3 \pm 0.03	0.274 \pm 8e-5	89.6 \pm 0.17	60.7 \pm 0.14	0.228 \pm 1e-2
LA-NAM	79.6 \pm 0.01	34.8 \pm 0.04	0.264 \pm 5e-5	90.1 \pm 0.03	60.5 \pm 0.14	0.174 \pm 2e-4
EBM ₁₀	79.7 \pm 0.03	34.9 \pm 0.09	0.264 \pm 2e-4	90.5 \pm 0.04	61.1 \pm 0.23	0.173 \pm 4e-4
LA-NAM ₁₀	80.2 \pm 0.10	35.2 \pm 0.06	0.262 \pm 3e-4	90.1 \pm 0.01	60.5 \pm 0.20	0.174 \pm 4e-4
LightGBM	80.6 \pm 0.08	35.6 \pm 0.19	0.261 \pm 3e-4	90.7 \pm 0.00	61.6 \pm 0.00	0.172 \pm 0.00

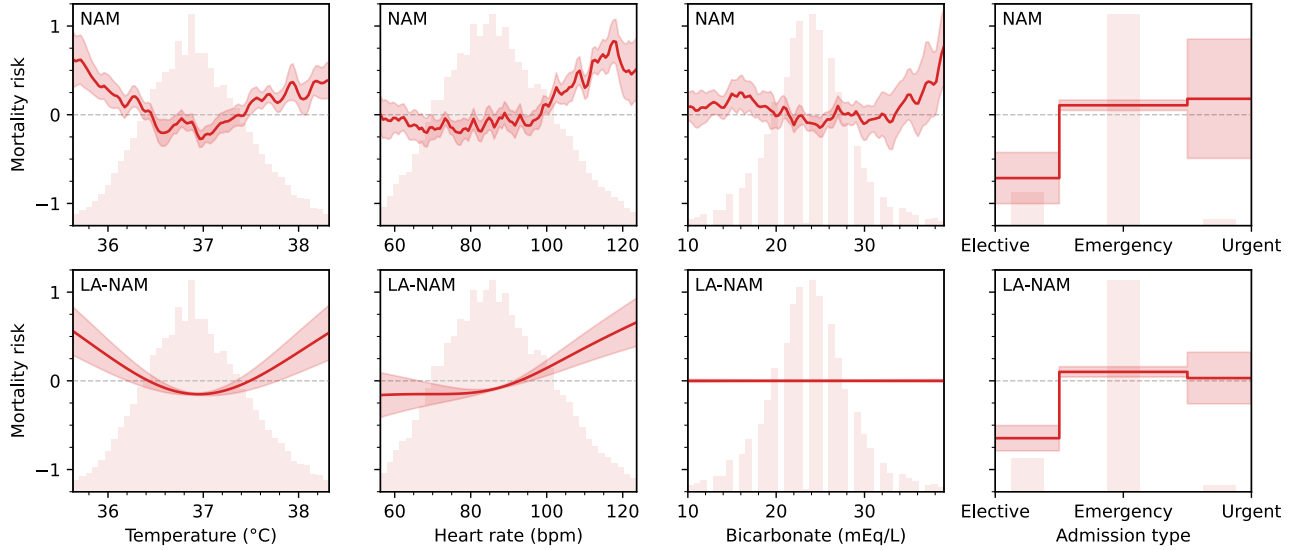


Figure 2: Risk of mortality and associated epistemic uncertainty (± 2 std. deviations) on the MIMIC-III mortality prediction task. The LA-NAM generates smoother feature curves, provides useful uncertainties, and ignores the uninformative feature.

hancing their modeling capacity. For these models, we also present results where we have employed their respective interaction detection methods to identify the top-10 feature pairs (LA-NAM₁₀ and EBM₁₀).

In Table 1, we report the negative log-likelihood averaged over test samples. The NAM and EBM do not provide an estimate of the observation noise in regression, so they are assigned a maximum likelihood fit using their training data. The LA-NAM consistently demonstrates competitive performance across multiple datasets. It tends to exhibit lower average negative log-likelihood, indicating better performance, compared to the NAM and performs comparatively well versus the EBM. LA-NAM₁₀, which refers to the fine-tuned model with top-10 feature interactions, almost always improves performance on re-

gression when compared to its non-feature-interactive counterpart and often reaches the performance of the fully-interacting LightGBM. Note that this might also be related to its ability to ignore uninformative features, which has been identified as a main weakness of neural networks on tabular data compared to tree-based methods (Grinsztajn et al., 2022). A wider set of models along with additional performance and calibration metrics are considered in Appendices B.5 and B.6.

4.3 Intensive Care Unit Mortality Prediction

To gain insights into the behavior of our method within a real-world clinical context, we investigate its performance in predicting patient mortality based on vital signs recorded 24 hours after admission into an inten-

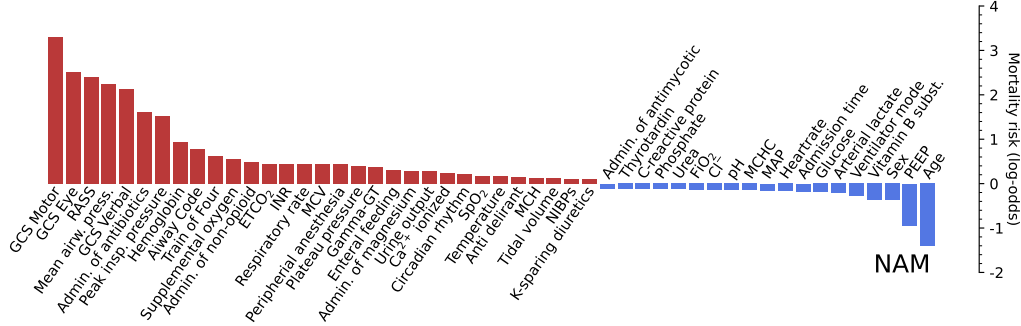


Figure 3: Local explanations for the risk of an example patient in the HiRID mortality task in the NAM. Features that contribute less than 0.1 to the log-odds magnitude of mortality risk are omitted. The model selects a large number of features and does not provide uncertainty estimates.

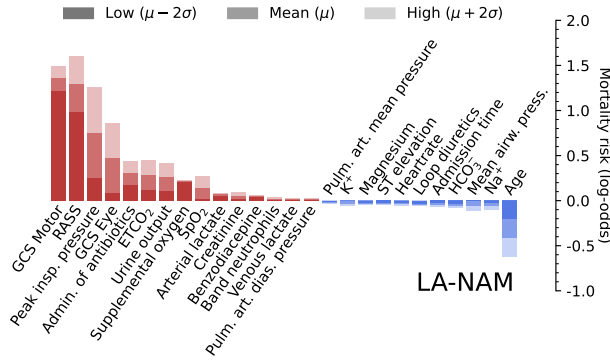


Figure 4: Local explanations from the LA-NAM for the same patient as in Fig. 3. Features whose credible intervals overlap with zero are omitted. The model selects far fewer features than the NAM and provides uncertainty estimates, further aiding its interpretation and facilitating its scrutiny.

sive care unit (ICU). To accomplish this, we utilize the MIMIC-III database (Johnson et al., 2016) and employ the pre-processing outlined by Lengerich et al. (2022). Additionally, we leverage the HiRID database (Faltys et al., 2021) and adopt the pre-processing methodology presented by Yèche et al. (2021). Notably, our objective extends beyond achieving competitive predictive performance: we aim to provide valuable insights into the underlying sources of risk within the ICU, ultimately enhancing interpretability and facilitating a clearer understanding of critical care dynamics.

Predictive performance. Table 2 presents a summary of the test performance achieved by the various methods. For the MIMIC-III dataset, a total of 14,960 patients were considered, with 2,231 held out as the test set. Similarly, the HiRID dataset is comprised of 27,347 patients, with 8,189 held out for test-

ing purposes. On these tasks, the LA-NAM demonstrates superior performance compared to the NAM in the key evaluation metrics of area under the ROC and precision-recall curve (AUROC and AUPRC), as well as average negative log-likelihood (NLL).² Fig. 2 showcases a subset of the recovered additive structure from the MIMIC-III dataset.³ In each subplot, the background displays a histogram depicting the distribution of feature values. Note that the NAM exhibits the same jumpy behavior observed in the synthetic example, which adversely affects interpretability, while the LA-NAM yields smoother curves, due to its optimized Bayesian prior. We find that the identified relationships of the displayed variables and risk by LA-NAM appear consistent with medical knowledge (personal communication with medical experts). We also find that the LA-NAM is effective in capturing and quantifying epistemic uncertainty, aligning with the presence or absence of sufficient samples.

Feature selection. This experiment also illustrates the ability of the LA-NAM to assess the relevance of features through selection of feature networks. Because of their linear dependency, both high bicarbonate levels and low anion gap are indicators of metabolic acidosis (Kraut and Madias, 2010). The LA-NAM has determined that the risk associated with bicarbonate can be adequately captured solely through the measurement of the anion gap. Consequently, the LA-NAM entirely disregards the bicarbonate feature, as demonstrated in Fig. 2. See Appendix B.2 for an ablation experiment confirming this.

Interpretability. The epistemic uncertainty and feature-selecting property of the LA-NAM significantly contribute to the effectiveness of the local explanations generated from it. This advantage becomes evident

²Calibration is also improved as shown in Appendix B.4.

³A complete visualization is provided in Appendix B.9.

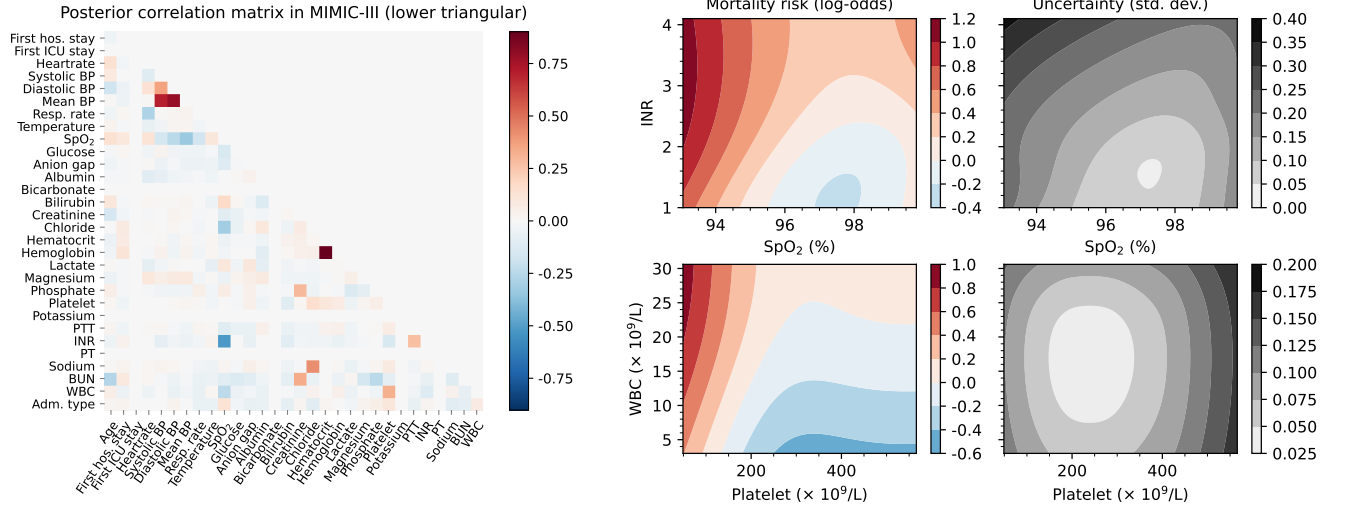


Figure 5: Feature interactions uncovered in the MIMIC-III dataset by the LA-NAM. (left) Last-layer posterior correlation matrix, used to select the most informative feature-interaction pairs. (right) Two selected example feature interactions, highlighting the interpretability of feature interactions in the LA-NAM, as well as the associated uncertainty estimates.

when examining Fig. 3 and Fig. 4, where we compare the breakdown of risk factors between the NAM and LA-NAM, respectively. We find that the LA-NAM selects a noticeably condensed and more concise and interpretable set of features. Moreover, it provides uncertainties in local explanations, which also brings valuable insight for interpretability by acknowledging the inherent variability and potential limitations of the model. In this case, it allows clinicians to gauge the reliability and robustness of the predicted risk factors, enabling more informed decision-making and facilitating trust in the model’s outputs.

Feature interactions. In addition to the first-order methods, both the EBM and LA-NAM were evaluated with fine-tuning using the top-10 feature interaction pairs (EBM₁₀ and LA-NAM₁₀ in Table 2). Incorporating these interactions led to significantly improved performance for the LA-NAM₁₀ on the MIMIC-III dataset, reaching competitive performance with the fully-interacting LightGBM gold standard. On the left side of Fig. 5, the last-layer correlation matrix for second-order interactions is presented, revealing the relationships between the different feature pair candidates for inclusion in the second-order fine-tuning stage. On the right side, specific interactions involving the risk factors of WBC and Platelet, as well as INR and SpO₂, are depicted. In particular, we show an increase in mortality risk for high white blood cell and low platelet counts as well as for elevated INR and low oxygen saturation. While the first interaction is characteristic of immune thrombocytopenia (Cooper

and Ghanima, 2019), a known risk factor for critically ill patients (Baughman et al., 1993; Trehel-Tursis et al., 2012), the second has not been studied in the literature. Hence, by enabling second-order interaction selection, LA-NAM may also help to discover new risk factors (of course, follow-up studies would be needed).

5 Conclusion

In this work, we have introduced a Bayesian adaptation of the widely-used neural additive model and derived a customized linearized Laplace approximation for inference. This approach allows for a natural decomposition of epistemic uncertainty across additive subnetworks, as well as implicit feature selection by optimizing the log-marginal likelihood. Our empirical results illustrate the robustness of our Laplace-approximated neural additive model (LA-NAM) against noise and uninformative features. Furthermore, when allowed to autonomously select its feature interactions, the LA-NAM demonstrates performance on par with fully interacting gold-standard baselines. The LA-NAM thus emerges as a compelling choice for safety-critical applications and as a tool for data-driven scientific discovery. Moreover, our work underscores the potential for future research at the intersection of interpretable machine learning and Bayesian inference. Overall, this work contributes to the vision of powerful, robust, yet transparent and understandable machine learning models. We hope that our work will inspire further advances in Bayesian additive models, marrying interpretability and probabilistic modeling.

Acknowledgments

We thank Ben Lengerich for providing us the pre-processed MIMIC-III dataset used in the paper. This project was supported by grant #2022-278 of the Strategic Focus Area “Personalized Health and Related Technologies (PHRT)” of the ETH Domain.

A.I. gratefully acknowledges funding by the Max Planck ETH Center for Learning Systems (CLS). V.F. was supported by a Branco Weiss Fellowship.

References

- Rishabh Agarwal, Levi Melnick, Nicholas Frosst, Xuezhou Zhang, Ben Lengerich, Rich Caruana, and Geoffrey E Hinton. Neural Additive Models: Interpretable Machine Learning with Neural Nets. In *Advances in Neural Information Processing Systems*, volume 34, pages 4699–4711. Curran Associates, Inc., 2021.
- Javier Antorán, David Janz, James U Allingham, Erik Daxberger, Riccardo Rb Barbano, Eric Nalisnick, and José Miguel Hernández-Lobato. Adapting the linearised laplace model evidence for modern deep learning. In *International Conference on Machine Learning*, pages 796–821. PMLR, 2022.
- Robert R Baughman, Elyse E Lower, Herbert C Flessa, and David J Tollerud. Thrombocytopenia in the intensive care unit. *Chest*, 104(4):1243–1247, 1993.
- Charles Blundell, Julien Cornebise, Koray Kavukcuoglu, and Daan Wierstra. Weight uncertainty in neural networks. In *ICML*, 2015.
- Leo Breiman and Jerome H. Friedman. Estimating Optimal Transformations for Multiple Regression and Correlation. *Journal of the American Statistical Association*, 80(391):580–598, September 1985. ISSN 0162-1459. doi: 10.1080/01621459.1985.10478157.
- Rich Caruana, Yin Lou, Johannes Gehrke, Paul Koch, Marc Sturm, and Noemie Elhadad. Intelligible Models for HealthCare: Predicting Pneumonia Risk and Hospital 30-day Readmission. In *Proceedings of the 21th ACM SIGKDD International Conference on Knowledge Discovery and Data Mining*, KDD ’15, pages 1721–1730, New York, NY, USA, August 2015. Association for Computing Machinery. ISBN 978-1-4503-3664-2. doi: 10.1145/2783258.2788613.
- Kamil Ciosek, Vincent Fortuin, Ryota Tomioka, Katja Hofmann, and Richard Turner. Conservative uncertainty estimation by fitting prior networks. In *International Conference on Learning Representations*, 2020.
- Nichola Cooper and Waleed Ghanima. Immune thrombocytopenia. *New England Journal of Medicine*, 381(10):945–955, 2019.
- G. Cybenko. Approximation by superpositions of a sigmoidal function. *Mathematics of Control, Signals and Systems*, 2(4):303–314, December 1989. ISSN 1435-568X. doi: 10.1007/BF02551274.
- Francesco D’Angelo and Vincent Fortuin. Repulsive deep ensembles are bayesian. *Advances in Neural Information Processing Systems*, 34:3451–3465, 2021.
- Francesco D’Angelo, Vincent Fortuin, and Florian Wenzel. On stein variational neural network ensembles. *arXiv preprint arXiv:2106.10760*, 2021.
- Erik Daxberger, Agustinus Kristiadi, Alexander Immer, Runa Eschenhagen, Matthias Bauer, and Philipp Hennig. Laplace Redux - Effortless Bayesian Deep Learning. In *Advances in Neural Information Processing Systems*, volume 34, pages 20089–20103. Curran Associates, Inc., 2021a.
- Erik Daxberger, Eric Nalisnick, James U Allingham, Javier Antorán, and José Miguel Hernández-Lobato. Bayesian deep learning via subnetwork inference. In *International Conference on Machine Learning*, pages 2510–2521. PMLR, 2021b.
- Martin Faltys, Marc Zimmermann, Xinrui Lyu, Matthias Hüser, Stephanie Hyland, Gunnar Rätsch, and Tobias Merz. Hirid, a high time-resolution icu dataset (version 1.1.1). *PhysioNet*, 2021.
- Andrew YK Foong, Yingzhen Li, José Miguel Hernández-Lobato, and Richard E Turner. ‘in-between’uncertainty in bayesian neural networks. *arXiv preprint arXiv:1906.11537*, 2019.
- Vincent Fortuin. Priors in bayesian deep learning: A review. *International Statistical Review*, 90(3):563–591, 2022.
- Vincent Fortuin, Adrià Garriga-Alonso, Mark van der Wilk, and Laurence Aitchison. Bnnpriors: A library for bayesian neural network inference with different prior distributions. *Software Impacts*, 9:100079, 2021.
- Vincent Fortuin, Adrià Garriga-Alonso, Sebastian W Ober, Florian Wenzel, Gunnar Ratsch, Richard E Turner, Mark van der Wilk, and Laurence Aitchison. Bayesian neural network priors revisited. In *International Conference on Learning Representations*, 2022.
- Jerome H. Friedman. Greedy Function Approximation: A Gradient Boosting Machine. *The Annals of Statistics*, 29(5):1189–1232, 2001. ISSN 0090-5364.
- Yarin Gal and Zoubin Ghahramani. Dropout as a Bayesian approximation: Representing model uncertainty in deep learning. In *ICML*, 2016.

- Adrià Garriga-Alonso and Vincent Fortuin. Exact Langevin dynamics with stochastic gradients. *arXiv preprint arXiv:2102.01691*, 2021.
- Gene H. Golub, Michael Heath, and Grace Wahba. Generalized Cross-Validation as a Method for Choosing a Good Ridge Parameter. *Technometrics*, 21(2):215–223, May 1979. ISSN 0040-1706, 1537-2723. doi: 10.1080/00401706.1979.10489751.
- Alex Graves. Practical variational inference for neural networks. In *NIPS*, 2011.
- Léo Grinsztajn, Edouard Oyallon, and Gaël Varoquaux. Why do tree-based models still outperform deep learning on tabular data? *arXiv preprint arXiv:2207.08815*, 2022.
- Sebastian Gruber and Florian Buettner. Better uncertainty calibration via proper scores for classification and beyond. *Advances in Neural Information Processing Systems*, 35:8618–8632, 2022.
- Chuan Guo, Geoff Pleiss, Yu Sun, and Kilian Q Weinberger. On calibration of modern neural networks. In *International conference on machine learning*, pages 1321–1330. PMLR, 2017.
- Trevor Hastie and Robert Tibshirani. *Generalized Additive Models*. Chapman & Hall/CRC, Boca Raton, Fla, 1999. ISBN 978-0-412-34390-2.
- Bobby He, Balaji Lakshminarayanan, and Yee Whye Teh. Bayesian deep ensembles via the neural tangent kernel. *Advances in neural information processing systems*, 33:1010–1022, 2020.
- Dan Hendrycks and Kevin Gimpel. Gaussian error linear units (gelus). *arXiv preprint arXiv:1606.08415*, 2016.
- Alexander Immer, Matthias Bauer, Vincent Fortuin, Gunnar Rätsch, and Mohammad Emtiyaz Khan. Scalable marginal likelihood estimation for model selection in deep learning. In *ICML*, 2021a.
- Alexander Immer, Maciej Korzepa, and Matthias Bauer. Improving predictions of Bayesian neural nets via local linearization. In *Proceedings of The 24th International Conference on Artificial Intelligence and Statistics*, pages 703–711. PMLR, March 2021b.
- Alexander Immer, Lucas Torroba Hennigen, Vincent Fortuin, and Ryan Cotterell. Probing as quantifying inductive bias. In *Proceedings of the 60th Annual Meeting of the Association for Computational Linguistics (Volume 1: Long Papers)*, pages 1839–1851, 2022a.
- Alexander Immer, Tycho FA van der Ouderaa, Vincent Fortuin, Gunnar Rätsch, and Mark van der Wilk. Invariance learning in deep neural networks with differentiable Laplace approximations. In *NeurIPS*, 2022b.
- Alexander Immer, Tycho FA Van Der Ouderaa, Mark Van Der Wilk, Gunnar Ratsch, and Bernhard Schölkopf. Stochastic marginal likelihood gradients using neural tangent kernels. In *International Conference on Machine Learning*, pages 14333–14352. PMLR, 2023.
- Pavel Izmailov, Dmitrii Podoprikin, Timur Garipov, Dmitry Vetrov, and Andrew Gordon Wilson. Averaging weights leads to wider optima and better generalization. In *34th Conference on Uncertainty in Artificial Intelligence 2018, UAI 2018*, pages 876–885, 2018.
- Pavel Izmailov, Sharad Vikram, Matthew D Hoffman, and Andrew Gordon Wilson. What are Bayesian neural network posteriors really like? In *ICML*, 2021.
- Alistair E. W. Johnson, Tom J. Pollard, Lu Shen, Liwei H. Lehman, Mengling Feng, Mohammad Ghassemi, Benjamin Moody, Peter Szolovits, Leo Anthony Celi, and Roger G. Mark. MIMIC-III, a freely accessible critical care database. *Scientific Data*, 3(1):160035, May 2016. ISSN 2052-4463. doi: 10.1038/sdata.2016.35.
- Laurent Valentin Jospin, Hamid Laga, Farid Bousaid, Wray Buntine, and Mohammed Bennamoun. Hands-on bayesian neural networks - a tutorial for deep learning users. *IEEE Computational Intelligence Magazine*, 17(2):29–48, 2022.
- Guolin Ke, Qi Meng, Thomas Finley, Taifeng Wang, Wei Chen, Weidong Ma, Qiwei Ye, and Tie-Yan Liu. LightGBM: A Highly Efficient Gradient Boosting Decision Tree. In *Advances in Neural Information Processing Systems*, volume 30. Curran Associates, Inc., 2017.
- Mohammad Khan, Didrik Nielsen, Voot Tangkaratt, Wu Lin, Yarin Gal, and Akash Srivastava. Fast and scalable Bayesian deep learning by weight-perturbation in Adam. In *ICML*, 2018.
- Mohammad Emtiyaz Khan, Alexander Immer, Ehsan Abedi, and Maciej Korzepa. Approximate inference turns deep networks into Gaussian processes. In *NeurIPS*, 2019.
- Diederik P Kingma and Jimmy Ba. Adam: A method for stochastic optimization. *arXiv preprint arXiv:1412.6980*, 2014.
- Diederik P Kingma, Tim Salimans, and Max Welling. Variational dropout and the local reparameterization trick. In *Advances in Neural Information Processing Systems 28*, 2015.

- Jeffrey A. Kraut and Nicolaos E. Madias. Metabolic acidosis: Pathophysiology, diagnosis and management. *Nature Reviews Nephrology*, 6(5):274–285, May 2010. ISSN 1759-507X. doi: 10.1038/nrneph.2010.33.
- Jeffrey A. Kraut and Nicolaos E. Madias. Treatment of acute metabolic acidosis: A pathophysiologic approach. *Nature Reviews. Nephrology*, 8(10):589–601, October 2012. ISSN 1759-507X. doi: 10.1038/nrneph.2012.186.
- Volodymyr Kuleshov, Nathan Fenner, and Stefano Ermon. Accurate uncertainties for deep learning using calibrated regression. In *International conference on machine learning*, pages 2796–2804. PMLR, 2018.
- Balaji Lakshminarayanan, Alexander Pritzel, and Charles Blundell. Simple and scalable predictive uncertainty estimation using deep ensembles. In *NIPS*, 2017.
- Pierre Simon Laplace. Mémoire sur la probabilité des causes par les évènements. In *Mémoires de l’Académie Royale Des Sciences de Paris (Savants Étrangers)*, volume 6, pages 621–656. 1774.
- Benjamin J. Lengerich, Rich Caruana, Mark E. Nunnally, and Manolis Kellis. Death by Round Numbers: Glass-Box Machine Learning Uncovers Biases in Medical Practice, November 2022.
- Yin Lou, Rich Caruana, and Johannes Gehrke. Intelligible models for classification and regression. In *Proceedings of the 18th ACM SIGKDD International Conference on Knowledge Discovery and Data Mining*, KDD ’12, pages 150–158, New York, NY, USA, August 2012. Association for Computing Machinery. ISBN 978-1-4503-1462-6. doi: 10.1145/2339530.2339556.
- Yin Lou, Rich Caruana, Johannes Gehrke, and Giles Hooker. Accurate intelligible models with pairwise interactions. In *Proceedings of the 19th ACM SIGKDD International Conference on Knowledge Discovery and Data Mining*, KDD ’13, pages 623–631, New York, NY, USA, August 2013. Association for Computing Machinery. ISBN 978-1-4503-2174-7. doi: 10.1145/2487575.2487579.
- Christos Louizos and Max Welling. Structured and efficient variational deep learning with matrix Gaussian posteriors. In *ICML*, 2016.
- Zhou Lu, Hongming Pu, Feicheng Wang, Zhiqiang Hu, and Liwei Wang. The Expressive Power of Neural Networks: A View from the Width. In *Advances in Neural Information Processing Systems*, volume 30. Curran Associates, Inc., 2017.
- Mattias Lubner, Anton Thielmann, and Benjamin Säfken. Structural Neural Additive Models: Enhanced Interpretable Machine Learning, February 2023.
- Scott M Lundberg and Su-In Lee. A Unified Approach to Interpreting Model Predictions. In *Advances in Neural Information Processing Systems*, volume 30. Curran Associates, Inc., 2017.
- David J. C. MacKay. Bayesian model comparison and backprop nets. In J. Moody, S. Hanson, and R.P. Lippmann, editors, *Advances in Neural Information Processing Systems*, volume 4. Morgan-Kaufmann, 1991.
- David J. C. MacKay. A practical Bayesian framework for backpropagation networks. *Neural Computation*, 4(3), 1992.
- David J. C. MacKay. Bayesian nonlinear modeling for the prediction competition. *ASHRAE transactions*, 100(2):1053–1062, 1994.
- Wesley J Maddox, Pavel Izmailov, Timur Garipov, Dmitry P Vetrov, and Andrew Gordon Wilson. A simple baseline for Bayesian uncertainty in deep learning. In *NeurIPS*, 2019.
- Vitaly Maiorov and Allan Pinkus. Lower bounds for approximation by MLP neural networks. *Neurocomputing*, 25(1):81–91, April 1999. ISSN 0925-2312. doi: 10.1016/S0925-2312(98)00111-8.
- James Martens and Roger Grosse. Optimizing Neural Networks with Kronecker-factored Approximate Curvature. In *International conference on machine learning*, pages 2408–2417. PMLR, 2015.
- Seth Nabarro, Stoil Kanev, Adrià Garriga-Alonso, Vincent Fortuin, Mark van der Wilk, and Laurence Aitchison. Data augmentation in bayesian neural networks and the cold posterior effect. In *Uncertainty in Artificial Intelligence*, pages 1434–1444. PMLR, 2022.
- Radford M Neal. Bayesian learning via stochastic dynamics. In *Advances in neural information processing systems*, pages 475–482, 1993.
- Radford M Neal. *Bayesian Learning for Neural Networks*. PhD thesis, University of Toronto, 1995.
- Radford M Neal et al. MCMC using Hamiltonian dynamics. *Handbook of Markov Chain Monte Carlo*, 2(11), 2011.
- Harsha Nori, Samuel Jenkins, Paul Koch, and Rich Caruana. InterpretML: A Unified Framework for Machine Learning Interpretability, September 2019.
- Kazuki Osawa, Siddharth Swaroop, Mohammad Emtiyaz E Khan, Anirudh Jain, Runa Eschenhagen, Richard E Turner, and Rio Yokota. Practical deep learning with Bayesian principles. In *NeurIPS*, 2019.

- F. Pedregosa, G. Varoquaux, A. Gramfort, V. Michel, B. Thirion, O. Grisel, M. Blondel, P. Prettenhofer, R. Weiss, V. Dubourg, J. Vanderplas, A. Passos, D. Cournapeau, M. Brucher, M. Perrot, and E. Duchesnay. Scikit-learn: Machine learning in Python. *Journal of Machine Learning Research*, 12: 2825–2830, 2011.
- Luisa Pumplun, Mariska Fecho, Nihal Wahl, Felix Peters, and Peter Buxmann. Adoption of Machine Learning Systems for Medical Diagnostics in Clinics: Qualitative Interview Study. *Journal of Medical Internet Research*, 23(10):e29301, October 2021. doi: 10.2196/29301.
- Filip Radenovic, Abhimanyu Dubey, and Dhruv Mahajan. Neural Basis Models for Interpretability. *Advances in Neural Information Processing Systems*, 35:8414–8426, December 2022.
- Marco Tulio Ribeiro, Sameer Singh, and Carlos Guestrin. “Why Should I Trust You?”: Explaining the Predictions of Any Classifier. In *Proceedings of the 22nd ACM SIGKDD International Conference on Knowledge Discovery and Data Mining*, KDD ’16, pages 1135–1144, New York, NY, USA, August 2016. Association for Computing Machinery. ISBN 978-1-4503-4232-2. doi: 10.1145/2939672.2939778.
- Hippolyt Ritter, Aleksandar Botev, and David Barber. A Scalable Laplace Approximation for Neural Networks. In *6th International Conference on Learning Representations, ICLR 2018-Conference Track Proceedings*, volume 6. International Conference on Representation Learning, 2018.
- Jonas Rothfuss, Vincent Fortuin, Martin Josifoski, and Andreas Krause. Pacoh: Bayes-optimal meta-learning with pac-guarantees. In *International Conference on Machine Learning*, pages 9116–9126. PMLR, 2021.
- Jonas Rothfuss, Martin Josifoski, Vincent Fortuin, and Andreas Krause. Pac-bayesian meta-learning: From theory to practice. *arXiv preprint arXiv:2211.07206*, 2022.
- Cynthia Rudin. Stop explaining black box machine learning models for high stakes decisions and use interpretable models instead. *Nature Machine Intelligence*, 1(5):206–215, 2019.
- Pola Schwöbel, Martin Jørgensen, Sebastian W Ober, and Mark Van Der Wilk. Last layer marginal likelihood for invariance learning. In *International Conference on Artificial Intelligence and Statistics*, pages 3542–3555. PMLR, 2022.
- Daniel Servén, Charlie Brummitt, Hassan Abedi, and hlink. pyGAM: Generalized Additive Models in Python. Zenodo, October 2018.
- Mrinank Sharma, Tom Rainforth, Yee Whye Teh, and Vincent Fortuin. Incorporating unlabelled data into bayesian neural networks. *arXiv preprint arXiv:2304.01762*, 2023.
- Anton Thielmann, René-Marcel Kruse, Thomas Kneib, and Benjamin Säfen. Neural Additive Models for Location Scale and Shape: A Framework for Interpretable Neural Regression Beyond the Mean, January 2023.
- Michael E Tipping. Sparse bayesian learning and the relevance vector machine. *Journal of machine learning research*, 1(Jun):211–244, 2001.
- Virginie Trehel-Tursis, Virginie Louvain-Quintard, Youssef Zarrouki, Audrey Imbert, Sylvie Doubine, and François Stéphan. Clinical and biologic features of patients suspected or confirmed to have heparin-induced thrombocytopenia in a cardiothoracic surgical icu. *Chest*, 142(4):837–844, 2012.
- Michael Tsang, Dehua Cheng, and Yan Liu. Detecting Statistical Interactions from Neural Network Weights, February 2018.
- Tycho FA van der Ouderaa and Mark van der Wilk. Learning invariant weights in neural networks. In *Uncertainty in Artificial Intelligence*, pages 1992–2001. PMLR, 2022.
- Michael Veale, Max Van Kleek, and Reuben Binns. Fairness and Accountability Design Needs for Algorithmic Support in High-Stakes Public Sector Decision-Making. In *Proceedings of the 2018 CHI Conference on Human Factors in Computing Systems*, CHI ’18, pages 1–14, New York, NY, USA, April 2018. Association for Computing Machinery. doi: 10.1145/3173574.3174014.
- Grace Wahba. Bayesian “Confidence Intervals” for the Cross-Validated Smoothing Spline. *Journal of the Royal Statistical Society: Series B (Methodological)*, 45(1):133–150, 1983. ISSN 2517-6161. doi: 10.1111/j.2517-6161.1983.tb01239.x.
- Ziyu Wang, Tongzheng Ren, Jun Zhu, and Bo Zhang. Function space particle optimization for bayesian neural networks. In *International Conference on Learning Representations*, 2019.
- Max Welling and Yee W Teh. Bayesian learning via stochastic gradient langevin dynamics. In *ICML*, 2011.
- David Widmann, Fredrik Lindsten, and Dave Zachariah. Calibration tests beyond classification. *arXiv preprint arXiv:2210.13355*, 2022.
- Andrew Gordon Wilson and Pavel Izmailov. Bayesian deep learning and a probabilistic perspective of generalization. In *NeurIPS*, 2020.

Shiyun Xu, Zhiqi Bu, Pratik Chaudhari, and Ian J. Barnett. Sparse Neural Additive Model: Interpretable Deep Learning with Feature Selection via Group Sparsity, February 2022.

Zebin Yang, Aijun Zhang, and Agus Sudjianto. GAMINet: An Explainable Neural Network based on Generalized Additive Models with Structured Interactions. *Pattern Recognition*, 120:108192, December 2021. ISSN 0031-3203. doi: 10.1016/j.patcog.2021.108192.

Hugo Yèche, Rita Kuznetsova, Marc Zimmermann, Matthias Hüser, Xinrui Lyu, Martin Faltys, and Gunnar Rätsch. HiRID-ICU-Benchmark — A Comprehensive Machine Learning Benchmark on High-resolution ICU Data. *Proceedings of the Neural Information Processing Systems Track on Datasets and Benchmarks*, 1, December 2021.

Improving Neural Additive Models with Bayesian Principles (Appendix)

A Additional Theoretical Results and Discussion

In this section, we provide additional details on the derivation of our approximate posterior for Bayesian NAMs and discuss in further detail the interaction detection procedure and theoretical computational bounds.

A.1 Feature Network Independence

The approximate posterior defined in Eq. (7) results in feature networks that are mutually independent due to the block-diagonal structure of the covariance matrix. This independence is needed for the decomposition of the predictive variance in Eq. (12). We elaborate here on the motivation behind this independence assumption.

As a thought experiment, suppose we wanted to find estimates of two variable terms b_1 and b_2 , such that their sum is equal to some constant C . We also desire that neither term b_1 or b_2 dominate the other so that they are roughly equally balanced. One possible setup for finding a *maximum a posteriori* (MAP) estimate of b_1 and b_2 could be to design a cost function $L(b_1, b_2)$ where the MAP solution is a minimizer,

$$p(b_1, b_2) = \mathcal{N}([b_1, b_2]^\top; \mathbf{0}, \lambda^{-1}\mathbf{I}), \quad p(C | b_1, b_2) = \mathcal{N}(C; b_1 + b_2, 1), \quad (\text{A.1})$$

$$\log p(b_1, b_2 | C) \propto \log p(C | b_1, b_2) + \log p(b_1, b_2) \quad (\text{A.2})$$

$$\propto -(b_1 + b_2 - C)^2 - \lambda(b_1^2 + b_2^2) \stackrel{\text{def}}{=} -L(b_1, b_2). \quad (\text{A.3})$$

For illustrative purposes, we set $C = 20$ and $\lambda = 0.01$. In the left side of Fig. A.1, we visualize the cost function values $L(b_1, b_2)$ and highlight the MAP solution as a white cross. Now, suppose we are interested in finding an approximate posterior distribution for b_1 and b_2 with a Laplace approximation centered at the MAP estimate. When we treat b_1 and b_2 as jointly dependent variables, we obtain the Gaussian approximate posterior distribution depicted on the right side of Fig. A.1.

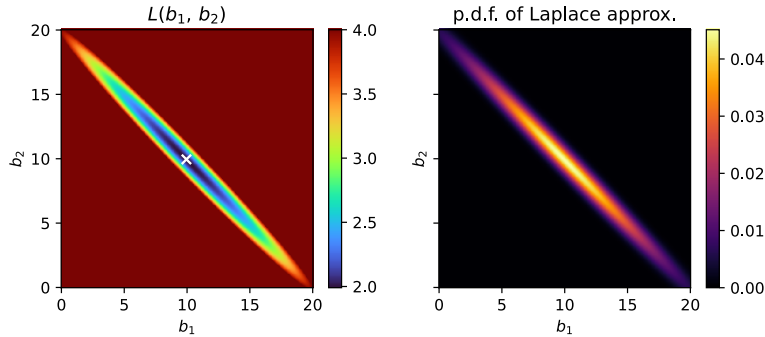


Figure A.1: Laplace approximation of the illustrative example in Appendix A.1. ($C = 20$, $\lambda = 0.01$)

In this approximation, b_1 and b_2 exhibit strong anti-correlation. This can be attributed to the observation that adjusting b_1 by some amount Δ can be accounted for by adjusting b_2 by $-\Delta$, since $b_1 + b_2 = (b_1 + \Delta) + (b_2 - \Delta)$. Within the realm of Bayesian NAMs, this property is considered undesirable. Ideally, we want the credible intervals for a feature network f_d to solely reflect changes in its shape, without being influenced by vertical translations of other feature networks. To circumvent the scenario illustrated above, one can adopt a strategy where b_1 and b_2 are treated as independent variables. This involves performing a first Laplace approximation for

b_1 while keeping b_2 fixed, followed by a separate Laplace approximation for b_2 keeping b_1 fixed. In our model, this is ensured by performing separate Laplace approximations for each feature network.

Nonetheless, the true posterior may contain strong statistical dependency across the feature networks. Therefore, for feature pairs which demonstrate high mutual information (Appendix A.2.1) or exhibit significant improvement on the marginal likelihood bound (Appendix A.2.2), we suggest to introduce second-order joint feature networks. The purpose of these networks is to explicitly capture these dependencies in the resulting fine-tuned model.

A.2 Feature Interaction Selection

In this section, we expand on the feature interaction selection based on the mutual information and also provide an alternative selection procedure which is phrased as model selection and optimization of the marginal likelihood.

A.2.1 Feature Interaction via Mutual Information

To select feature interactions, we consider the mutual information (MI) between the posteriors of feature networks. If the mutual information between θ_d and $\theta_{d'}$ is high, it is simultaneously high between the functional posteriors f_d and $f_{d'}$. This means that conditioning on the output of feature network f_d can provide information about the posterior of feature network $f_{d'}$, and therefore be an indication that a joint feature network for the interacting features could ultimately improve the LA-NAM fit. In a separate dense covariance matrix Laplace approximation, each candidate pair (d, d') has two marginal posteriors and a joint posterior. These are Gaussian distributions with corresponding covariance matrices $\Sigma_d, \Sigma_{d'}$, and $\Sigma_{d, d'}$. The mutual information can be approximated using

$$I(\theta_d; \theta_{d'}) \approx -\frac{1}{2} \log |\Sigma_{d, d'} (\Sigma_d \oplus \Sigma_{d'})^{-1}| = -\frac{1}{2} \log [|\Sigma_{d, d'}| |\Sigma_d^{-1}| |\Sigma_{d'}^{-1}|], \quad (\text{A.4})$$

where \oplus denotes block-diagonal concatenation. Constructing the full covariance matrix can be prohibitively expensive for a LA-NAM containing many feature networks. Instead, we can iteratively compute the covariance blocks $\Sigma_{d, d'}$ and determine the mutual information of each pair using Jacobians and precision matrices which are at most $2P \times 2P$ large (Daxberger et al., 2021b). Alternatively, we propose to use a last-layer approximation in Section 3.2.3 which turns the computation into $D \times D$ matrices and relies on scalar marginal variances.

For linearized Laplace approximations one can show that this is closely related to maximizing the mutual information of the posterior on f_d and $f_{d'}$ over the training set. In other words, how much information is gained about f_d when observing $f_{d'}$ and vice-versa. The joint posterior predictive on f_d and $f_{d'}$ is a Gaussian with a 2×2 covariance matrix per data point, meaning $N \times N$ marginal predictive covariance matrices \mathbf{S}_d and $\mathbf{S}_{d'}$, and a $2N \times 2N$ joint predictive covariance matrix $\mathbf{S}_{d, d'}$, when considering the entire training set. In similar fashion to Eq. (A.4), the mutual information of the functional posterior distribution can be determined by taking

$$I(\mathbf{f}_d; \mathbf{f}_{d'}) = -\frac{1}{2} \log |\mathbf{S}_{d, d'} (\mathbf{S}_d \oplus \mathbf{S}_{d'})^{-1}| = -\frac{1}{2} \log [|\mathbf{S}_{d, d'}| |\mathbf{S}_d^{-1}| |\mathbf{S}_{d'}^{-1}|]. \quad (\text{A.5})$$

Moreover, taking $\mathbf{J}_{d, d'} \in \mathbb{R}^{2N \times 2P}$ as the Jacobian matrix of $[f_d, f_{d'}]^\top$ with respect to $[\theta_d, \theta_{d'}]^\top$ over the training data, with brackets denoting concatenation, we can write the marginal and joint predictive covariances as

$$\mathbf{S}_{d, d'} = \mathbf{J}_{d, d'} \Sigma_{d, d'} \mathbf{J}_{d, d'}^\top \quad \text{and} \quad \mathbf{S}_d \oplus \mathbf{S}_{d'} = \mathbf{J}_{d, d'} (\Sigma_d \oplus \Sigma_{d'}) \mathbf{J}_{d, d'}^\top. \quad (\text{A.6})$$

Plugging Eq. (A.6) back into the mutual information in Eq. (A.5), we see that it is equivalent to the parametric mutual information in Eq. (A.4) when we have $N = P$ and full-rank Jacobians. This shows that the parametric mutual information can also be thought of as an approximation to the functional mutual information.

A.2.2 Feature Interaction as Model Selection

Alternatively, we can phrase the selection of feature interactions as model selection, thereby optimizing the marginal likelihood of the Bayesian model. Mathematically, we can achieve this by choosing the feature pairs that maximize the lower bound to the log-marginal likelihood which stems from the factorized block-diagonal posterior. Adding any feature interaction in the posterior will reduce the slack of the bound in Eq. (11) and we aim to choose the ones reducing it the most. For any feature pair (d, d') , taking $\mathbf{J}_i \in \mathbb{R}^{N \times P}$ as the Jacobian

matrix of f_i with respect to θ_i over training data, we can estimate the improvement on the bound by considering

$$\text{gain}(d, d') = \sum_{i \in \{d, d'\}} [\log |\underbrace{\mathbf{J}_i^\top \text{diag}[\boldsymbol{\gamma}] \mathbf{J}_i + \lambda_i \mathbf{I}}_{P \times P}|] - \log |\underbrace{\mathbf{J}_{d, d'}^\top \text{diag}[\boldsymbol{\gamma}] \mathbf{J}_{d, d'} + \lambda_d \mathbf{I} \oplus \lambda_{d'} \mathbf{I}}_{2P \times 2P}|] \quad (\text{A.7})$$

$$= \log |\mathbf{P}_d| + \log |\mathbf{P}_{d'}| - \log |\mathbf{P}_{d, d'}| = -\log [|\mathbf{P}_{d, d'}| |\mathbf{P}_d^{-1}| |\mathbf{P}_{d'}^{-1}|], \quad (\text{A.8})$$

where $\text{diag}[\boldsymbol{\gamma}]$ denotes a diagonal matrix containing $\gamma_1, \dots, \gamma_N$. This quantifies the extent to which the log-marginal likelihood of the LA-NAM is enhanced when accounting for the posterior interaction between feature networks f_d and $f_{d'}$. The gain heuristic is derived from subtracting the approximate log-marginal likelihood of the initial model from one where a joint feature network is added.

As with the mutual information procedure, one can simplify this into a scalar case, thus maximizing normalized joint precision values instead of correlations. This makes intuitive sense as well since the precision values can indicate pairwise independence when conditioning on all other variables, that is for all $d'' \notin \{d, d'\}$.

A.3 Computational Considerations and Complexities

We briefly discuss the complexity of the proposed method, taking both computation and storage of the various quantities in consideration. For simplicity, we assume a LA-NAM with D feature networks, each with fixed number of parameters P , even though in practice the number of parameters can vary among feature networks.

In order to compute the block-diagonal approximate posterior of Eq. (7) we must determine and invert a Laplace-GGN posterior precision matrix for each feature network, resulting in total complexity of $\mathcal{O}(DNP^2)$ and $\mathcal{O}(DP^3)$, respectively. Storage of the matrix can be done in $\mathcal{O}(DP^2)$ and computing its determinant in $\mathcal{O}(DP^3)$. This can be overly prohibitive for large numbers of parameters, but can be significantly alleviated by using a layer-wise Kronecker-factored approximation (KFAC-GGN; Martens and Grosse, 2015). Assuming an architecture with a single layer with hidden size $\mathcal{O}(\sqrt{P})$, KFAC-GGN reduces computation of the precision matrix to $\mathcal{O}(DNP)$ and its inversion to $\mathcal{O}(DP^{3/2})$. Further details are provided in Immer et al. (2021b).

A separate Laplace approximation is required for both of the proposed feature interaction selection methods. The approximate covariance matrix must contain off-diagonal blocks since both the mutual information and improvement on the log-marginal likelihood depend on joint covariance matrices for each candidate pair. One option is to perform sub-network Laplace inference (Daxberger et al., 2021b) in order to iteratively score the pairs, which equates to taking $D \cdot (D - 1) / 2$ separate Laplace approximations over $2P$ parameters. We propose instead to perform a last-layer approximation by only considering the D output weights of each feature network, which results in computation in $\mathcal{O}(ND^2)$, storage in $\mathcal{O}(D^2)$, and inversion for mutual information in $\mathcal{O}(D^3)$.

B Additional Results and Experiments

B.1 Comparison of Approximate Inference Methods

We provide a brief overview of alternative approximate inference methods which can be employed to quantify uncertainty of feature networks in Bayesian NAMs. Fig. B.1 displays the recovered functions and predictive intervals generated using these methods on the toy example of Section 4.1.

Deep ensembles (DE). The NAM of Agarwal et al. (2021) effectively operates as a deep ensemble (Lakshminarayanan et al., 2017) even though the authors do not explicitly present it as such. In our experiments, we found that ensembles of feature networks using ReLU and GELU activation tend to exhibit a collapse of diversity in function space, as can be seen in the two leftmost panels of Fig. B.1. D’Angelo and Fortuin (2021) also highlight this as a potential limitation of deep ensembles. The utilization of ExU activation partially restores diversity, hence our focus on this configuration when comparing the NAM to the LA-NAM.

Mean-field variational inference (MFVI). Variational inference can also be used to obtain independent approximate feature network posteriors. In early experiments, we tested the Bayes-by-Backprop (*BbB*) procedure of Blundell et al. (2015) and found that the method required significant manual tuning since the feature networks tended to either severely underfit the functions or the uncertainty. MFVI also yields log-marginal likelihood estimates, however their use in gradient-optimization of neural network hyperparameters appears to be limited.

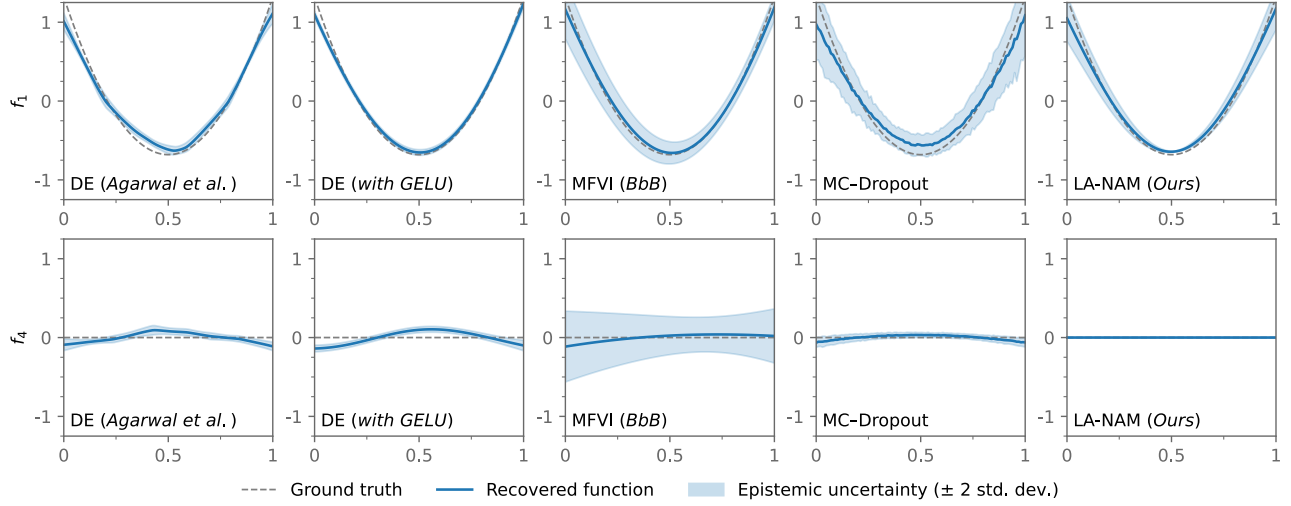


Figure B.1: Comparison of approximate inference methods for Bayesian NAMs trained on the synthetic dataset of Section 4.1. All feature networks use a single layer of 64 GELU units with the exception of the leftmost model, “DE (Agarwal et al.)”, which uses 64-64-32 ReLU units.

MC-Dropout. Dropout (Gal and Ghahramani, 2016) can be a simple way of introducing uncertainty awareness in the NAM but its Bayesian interpretation is not as straightforward as that of the Laplace approximation. It requires multiple forward passes for inference and does not provide an inherent mechanism for feature selection.

B.2 Ablation of the Anion Gap in MIMIC-III

The anion gap is a measure of the difference between the serum concentration of sodium and the serum concentrations of chloride and bicarbonate, i.e. $\text{anion gap} = [\text{Na}^+] - ([\text{Cl}^-] + [\text{HCO}_3^-])$.

Both low bicarbonate levels and thus high anion gap are indicators of acute metabolic acidosis. This is a known risk factor for intensive care mortality with very poor prognosis (Kraut and Madias, 2010, 2012). Fig. B.2 shows that the predicted mortality risk increases steadily as the anion gap grows but becomes uncertain above 20 mEq/L due to low sample size.

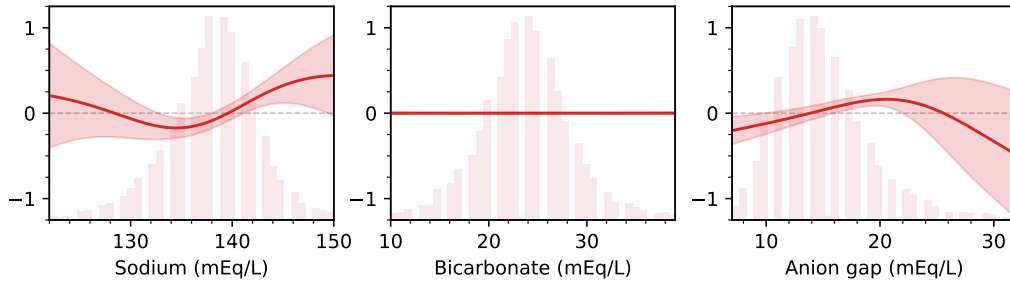


Figure B.2: Sodium, bicarbonate and anion gap mortality risk as predicted by the LA-NAM.

When presented with both anion gap and bicarbonate in the mortality risk dataset of Section 4.3, the LA-NAM uses high anion gap as a proxy for the risk of low bicarbonate. We confirm this visually by performing an ablation experiment in which the LA-NAM is re-trained with the feature network attending to the anion gap removed. Fig. B.3 shows that in the ablated model the anion gap risk is moved into the low levels for bicarbonate. The bicarbonate risk increases below 20 mEq/L and becomes uncertain around 15 mEq/L.

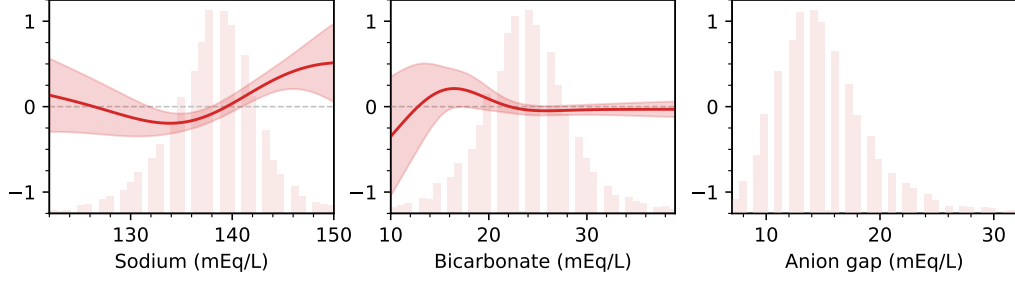


Figure B.3: Sodium and bicarbonate mortality risk with anion gap feature network ablated.

B.3 Ablation of the Activation Function

In Fig. B.4 and Table B.1, we progressively ablate the feature network depth and activation function of the NAM to match ours. Shallow networks and GELU activation encourage smoother fits at the expense of worse predictive uncertainty and performance. This is not a concern for the LA-NAM when applied to the same architecture

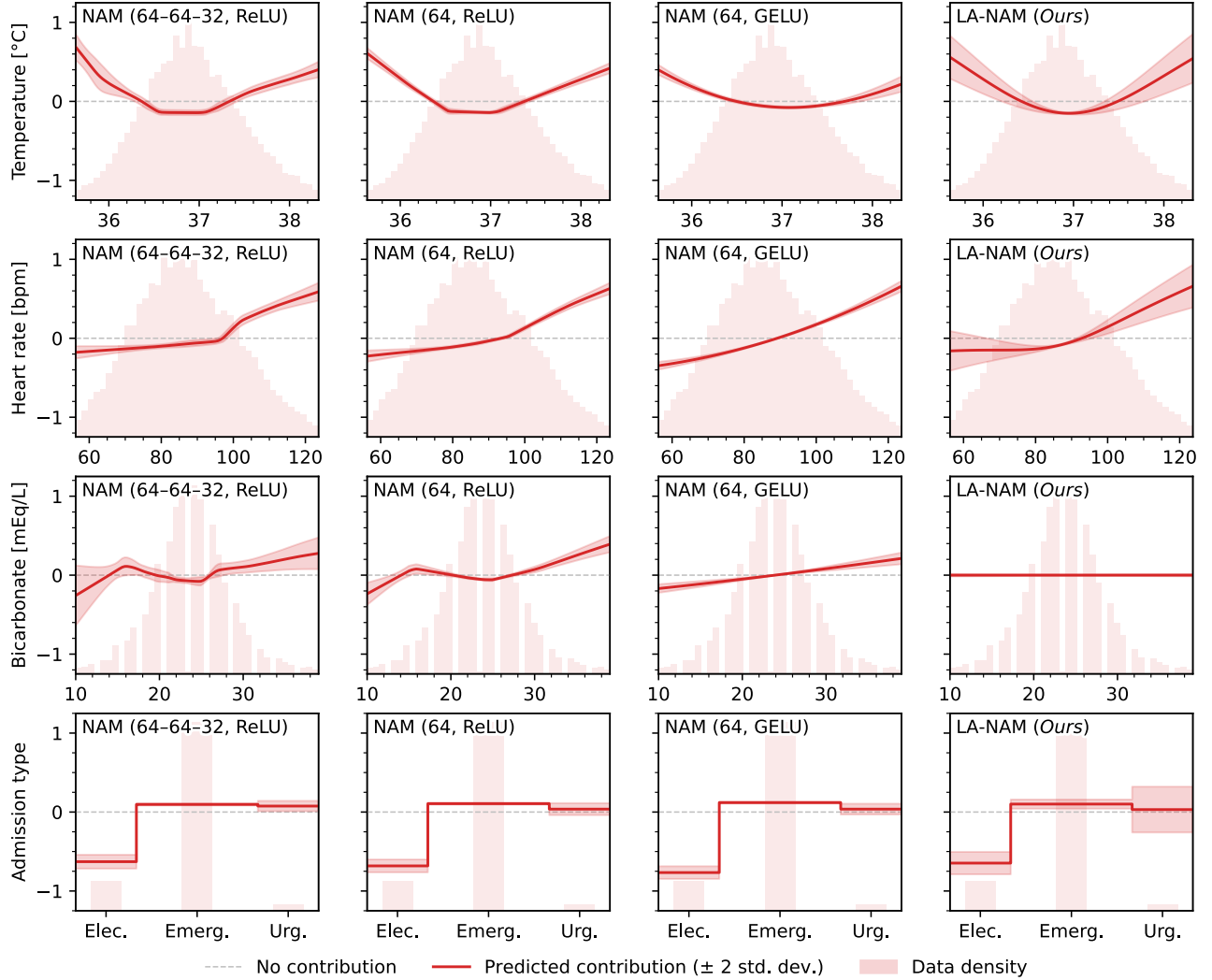


Figure B.4: Progressive ablation of the feature network depth and activation function on the MIMIC-III dataset of Section 4.3. Feature network architecture is in parentheses. Ours is a single layer of 64 GELU units.

Table B.1: Mean and standard errors over 5 runs for the performance of the ablated models shown in Fig. B.4.

MIMIC-III Performance	AUROC (\uparrow)	AUPRC (\uparrow)	NLL (\downarrow)
NAM (64-64-32, ReLU)	78.89 (± 0.04)	34.30 (± 0.04)	0.2669 ($\pm 2e-4$)
NAM (64, ReLU)	79.02 (± 0.02)	34.28 (± 0.02)	0.2665 ($\pm 1e-4$)
NAM (64, GELU)	77.54 (± 0.02)	34.10 (± 0.02)	0.2699 ($\pm 1e-4$)
LA-NAM (64, GELU)	79.58 (± 0.01)	34.77 (± 0.04)	0.2644 ($\pm 1e-4$)

B.4 Calibration on the ICU Mortality Prediction Tasks

We assess the calibration of the NAM and LA-NAM predictions on the ICU mortality tasks of Section 4.3. Following the protocol introduced by Ciosek et al. (2020), we present the accuracy as a function of subsets of retained test points in Fig. B.5. The points are first sorted based on the confidence level of the models and then progressively added to the subset to determine a rolling accuracy. The median of the rolling accuracy curves for 5 independent runs is shown. On the MIMIC-III dataset, the LA-NAM demonstrates superior calibration compared to the NAM, and it exhibits similar calibration on the significantly larger HiRID ICU dataset. Importantly, the incorporation of feature interactions does not seem to adversely harm calibration.

In Table B.2, we report mean calibration errors and their respective standard errors over the same 5 independent runs. We provide both the standard expected calibration error (ECE) of Guo et al. (2017), and the root Brier score (RBS), a proper calibration error put forward by Gruber and Buettner (2022). Bold values signify best calibration within one standard error, with the exception of LA-NAM₁₀ where bold indicates on par or better calibration compared to the first-order methods.

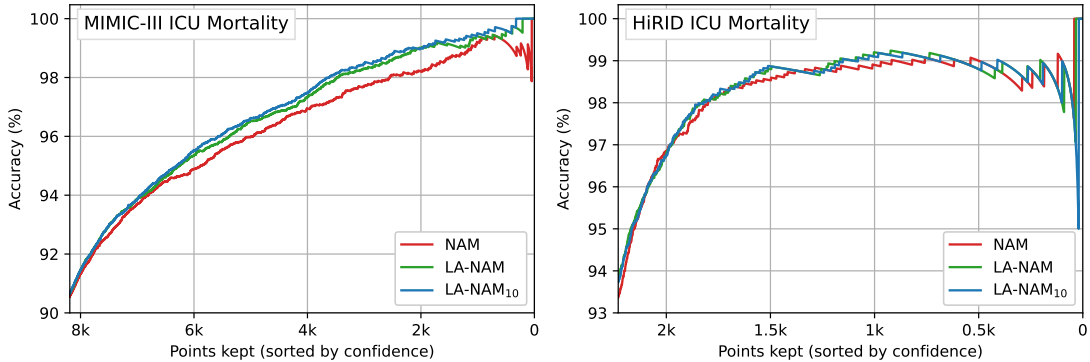


Figure B.5: Calibration curves of the mortality prediction models showing the relationship between uncertainty (horizontal axis) and accuracy (vertical axis). In well-calibrated models, accuracy should increase monotonically.

Table B.2: Calibration errors over the 5 runs of the mortality models assessed in Fig. B.5.

Model	NAM		LA-NAM		LA-NAM ₁₀	
	ECE (\downarrow)	RBS (\downarrow)	ECE (\downarrow)	RBS (\downarrow)	ECE (\downarrow)	RBS (\downarrow)
MIMIC-III ICU Mortality	0.019 $\pm 3.7e-4$	0.279 $\pm 1.2e-5$	0.009 $\pm 1.6e-4$	0.275 $\pm 2.5e-5$	0.009 $\pm 6.7e-4$	0.275 $\pm 9.6e-5$
HiRID ICU Mortality	0.029 $\pm 2.4e-3$	0.223 $\pm 3.7e-4$	0.009 $\pm 3.3e-4$	0.219 $\pm 1.6e-4$	0.011 $\pm 4.9e-4$	0.219 $\pm 2.3e-4$

B.5 Additional Results on UCI Datasets

In this section, we report the mean performance and standard errors for additional models and metrics over the 5-fold cross-validation UCI benchmarks of Section 4.2. Bolded values indicate best performance within additive models, and green or red an improvement or decrease beyond one standard error when second-order interactions are added. In addition to the models of Table 1, we give performance for linear and logistic regression, the smoothing-spline GAM, and the LA-NAM with 10 interactions selected using the improvement to the marginal likelihood lower bound which is discussed in Appendix A.2.2 and denoted as LA-NAM₁₀^{*}, instead of the MI-based selection presented in Section 3.2.3.

Table B.3: Negative test log-likelihood on UCI regression (top) and classification (bottom). (Lower is better.)

Dataset	Linear	GAM	EBM	NAM	LA-NAM	EBM ₁₀	LA-NAM ₁₀	LA-NAM ₁₀ [*]	LightGBM
autopmg ($n = 392$)	2.59 \pm 0.06	2.43 \pm 0.09	2.64 \pm 0.10	2.69 \pm 0.16	2.46 \pm 0.08	2.99 \pm 0.29	2.45 \pm 0.09	2.41 \pm 0.08	2.53 \pm 0.07
concrete ($n = 1030$)	3.78 \pm 0.04	3.13 \pm 0.05	3.20 \pm 0.12	3.46 \pm 0.12	3.25 \pm 0.03	3.53 \pm 0.20	3.18 \pm 0.04	3.14 \pm 0.03	3.09 \pm 0.09
energy ($n = 768$)	2.46 \pm 0.02	1.46 \pm 0.02	1.46 \pm 0.02	1.48 \pm 0.02	1.44 \pm 0.02	0.67 \pm 0.05	1.11 \pm 0.12	1.01 \pm 0.14	0.81 \pm 0.05
kin8nm ($n = 8192$)	-0.18 \pm 0.01	-0.20 \pm 0.01	-0.20 \pm 0.01	-0.18 \pm 0.01	-0.20 \pm 0.00	-0.34 \pm 0.01	-0.28 \pm 0.02	-0.29 \pm 0.02	-0.50 \pm 0.03
naval ($n = 11934$)	-3.72 \pm 0.01	-8.09 \pm 0.02	-3.15 \pm 0.00	-3.87 \pm 0.01	-7.24 \pm 0.01	-3.60 \pm 0.01	-7.44 \pm 0.07	-7.35 \pm 0.12	-5.19 \pm 0.01
power ($n = 9568$)	2.94 \pm 0.01	2.84 \pm 0.01	2.79 \pm 0.02	2.89 \pm 0.02	2.85 \pm 0.01	2.72 \pm 0.02	2.79 \pm 0.01	2.79 \pm 0.01	2.67 \pm 0.02
protein ($n = 45730$)	3.06 \pm 0.00	3.02 \pm 0.00	3.00 \pm 0.00	3.02 \pm 0.00	3.02 \pm 0.00	2.89 \pm 0.01	2.94 \pm 0.01	2.94 \pm 0.00	2.83 \pm 0.00
wine ($n = 1599$)	1.00 \pm 0.03	0.98 \pm 0.03	0.99 \pm 0.03	1.02 \pm 0.04	0.98 \pm 0.03	1.01 \pm 0.04	0.97 \pm 0.03	0.97 \pm 0.03	0.96 \pm 0.03
yacht ($n = 308$)	3.64 \pm 0.07	1.87 \pm 0.10	1.93 \pm 0.13	2.24 \pm 0.08	1.81 \pm 0.10	4.80 \pm 1.59	0.76 \pm 0.20	1.00 \pm 0.11	1.37 \pm 0.28
australian ($n = 690$)	0.35 \pm 0.02	0.35 \pm 0.04	0.33 \pm 0.03	0.38 \pm 0.04	0.34 \pm 0.03	0.32 \pm 0.04	0.34 \pm 0.03	0.35 \pm 0.03	0.31 \pm 0.03
breast ($n = 569$)	0.10 \pm 0.01	0.09 \pm 0.02	0.12 \pm 0.02	0.16 \pm 0.03	0.10 \pm 0.02	0.12 \pm 0.02	0.10 \pm 0.02	0.10 \pm 0.02	0.09 \pm 0.01
heart ($n = 270$)	0.39 \pm 0.04	0.43 \pm 0.08	0.40 \pm 0.02	0.41 \pm 0.04	0.33 \pm 0.02	0.41 \pm 0.03	0.33 \pm 0.03	0.34 \pm 0.03	0.39 \pm 0.04
ionosphere ($n = 351$)	0.33 \pm 0.03	0.27 \pm 0.02	0.23 \pm 0.02	0.31 \pm 0.04	0.25 \pm 0.04	0.22 \pm 0.02	0.27 \pm 0.03	0.27 \pm 0.03	0.19 \pm 0.03
parkinsons ($n = 195$)	0.33 \pm 0.02	0.36 \pm 0.02	0.28 \pm 0.05	0.29 \pm 0.04	0.26 \pm 0.03	0.36 \pm 0.12	0.25 \pm 0.03	0.25 \pm 0.03	0.22 \pm 0.03

Table B.4: Root mean squared error on UCI regression datasets. (Lower is better.)

Dataset	Linear	GAM	EBM	NAM	LA-NAM	EBM ₁₀	LA-NAM ₁₀	LA-NAM ₁₀ [*]	LightGBM
autopmg ($n = 392$)	3.18 \pm 0.18	2.70 \pm 0.20	2.98 \pm 0.11	2.94 \pm 0.19	2.77 \pm 0.18	2.86 \pm 0.15	2.72 \pm 0.19	2.66 \pm 0.17	2.96 \pm 0.13
concrete ($n = 1030$)	10.50 \pm 0.40	5.57 \pm 0.24	5.15 \pm 0.25	6.89 \pm 0.45	6.27 \pm 0.13	4.41 \pm 0.17	5.80 \pm 0.19	5.60 \pm 0.17	4.94 \pm 0.35
energy ($n = 768$)	2.84 \pm 0.05	1.04 \pm 0.02	1.04 \pm 0.02	1.06 \pm 0.02	1.04 \pm 0.02	0.47 \pm 0.02	0.76 \pm 0.08	0.68 \pm 0.09	0.52 \pm 0.02
kin8nm ($n = 8192$)	0.20 \pm 0.00	0.20 \pm 0.00	0.20 \pm 0.00	0.20 \pm 0.00	0.20 \pm 0.00	0.17 \pm 0.00	0.18 \pm 0.00	0.18 \pm 0.00	0.13 \pm 0.00
naval ($n = 11934$)	0.01 \pm 0.00	7e-5 \pm 2e-6	0.01 \pm 0.00	0.01 \pm 0.00	2e-4 \pm 2e-6	0.01 \pm 0.00	1e-4 \pm 1e-5	2e-4 \pm 2e-5	1e-3 \pm 6e-6
power ($n = 9568$)	4.56 \pm 0.06	4.15 \pm 0.06	3.89 \pm 0.06	4.34 \pm 0.06	4.18 \pm 0.06	3.62 \pm 0.06	3.93 \pm 0.06	3.94 \pm 0.06	3.39 \pm 0.06
protein ($n = 45730$)	5.19 \pm 0.01	4.94 \pm 0.01	4.84 \pm 0.01	4.98 \pm 0.01	4.94 \pm 0.01	4.36 \pm 0.02	4.58 \pm 0.02	4.57 \pm 0.02	4.09 \pm 0.01
wine ($n = 1599$)	0.65 \pm 0.02	0.65 \pm 0.01	0.64 \pm 0.02	0.64 \pm 0.02	0.64 \pm 0.02	0.62 \pm 0.01	0.64 \pm 0.02	0.64 \pm 0.02	0.62 \pm 0.02
yacht ($n = 308$)	9.09 \pm 0.54	1.51 \pm 0.16	1.56 \pm 0.16	2.20 \pm 0.15	1.45 \pm 0.17	0.68 \pm 0.09	0.72 \pm 0.13	0.81 \pm 0.09	0.79 \pm 0.11

Table B.5: Area under the ROC curve in percent on UCI classification datasets. (Higher is better.)

Dataset	Linear	GAM	EBM	NAM	LA-NAM	EBM ₁₀	LA-NAM ₁₀	LA-NAM ₁₀ [*]	LightGBM
australian ($n = 690$)	92.55 \pm 0.96	91.91 \pm 1.46	93.17 \pm 1.27	92.01 \pm 1.04	92.60 \pm 1.14	93.39 \pm 1.35	92.55 \pm 1.11	92.14 \pm 1.01	93.80 \pm 1.00
breast ($n = 569$)	99.60 \pm 0.24	99.40 \pm 0.35	99.24 \pm 0.19	98.97 \pm 0.38	99.45 \pm 0.21	99.35 \pm 0.21	99.42 \pm 0.21	99.39 \pm 0.28	99.30 \pm 0.30
heart ($n = 270$)	90.00 \pm 2.37	89.14 \pm 2.79	90.31 \pm 1.44	90.31 \pm 2.03	93.53 \pm 1.42	89.00 \pm 1.56	93.36 \pm 1.46	93.36 \pm 1.53	91.00 \pm 2.00
ionosphere ($n = 351$)	90.42 \pm 2.10	95.38 \pm 0.88	96.33 \pm 0.84	95.05 \pm 1.25	94.46 \pm 1.33	97.34 \pm 0.68	94.66 \pm 1.13	94.34 \pm 1.15	97.30 \pm 0.90
parkinsons ($n = 195$)	90.01 \pm 2.23	88.54 \pm 2.64	94.64 \pm 1.95	94.62 \pm 1.38	94.52 \pm 1.74	97.41 \pm 0.73	94.01 \pm 1.87	94.52 \pm 1.74	95.50 \pm 1.30

Table B.6: Area under the precision-recall curve in percent on UCI classification datasets. (Higher is better.)

Dataset	Linear	GAM	EBM	NAM	LA-NAM	EBM ₁₀	LA-NAM ₁₀	LA-NAM ₁₀ [*]	LightGBM
australian ($n = 690$)	91.17 \pm 0.76	91.09 \pm 1.17	91.82 \pm 1.41	90.01 \pm 1.21	92.08 \pm 1.22	92.12 \pm 1.39	91.93 \pm 1.33	91.68 \pm 1.20	92.80 \pm 1.30
breast ($n = 569$)	99.72 \pm 0.18	99.59 \pm 0.26	99.52 \pm 0.13	99.19 \pm 0.39	99.63 \pm 0.15	99.59 \pm 0.14	99.62 \pm 0.16	99.59 \pm 0.19	99.50 \pm 0.20
heart ($n = 270$)	88.52 \pm 2.98	87.77 \pm 3.72	88.71 \pm 1.88	89.08 \pm 2.83	92.58 \pm 1.78	87.85 \pm 1.94	92.56 \pm 1.85	92.51 \pm 1.92	89.10 \pm 3.20
ionosphere ($n = 351$)	91.05 \pm 2.19	97.16 \pm 0.60	97.44 \pm 0.72	96.28 \pm 1.08	95.44 \pm 1.19	98.21 \pm 0.52	95.11 \pm 1.32	94.87 \pm 1.36	98.10 \pm 0.70
parkinsons ($n = 195$)	96.73 \pm 0.76	95.90 \pm 1.25	98.09 \pm 0.83	98.14 \pm 0.50	98.15 \pm 0.60	99.20 \pm 0.23	98.04 \pm 0.59	98.18 \pm 0.59	98.40 \pm 0.50

B.6 Calibration on UCI Datasets

We also provide calibration errors and respective standard errors for the 5-fold UCI benchmarks in Tables B.7 and B.8. For the UCI classification datasets we reuse the metrics of Appendix B.4, namely the expected calibration error (ECE) of Guo et al. (2017) and the root Brier score (RBS) proposed by Gruber and Buettner (2022). In UCI regression, we provide the quantile error metric proposed by Kuleshov et al. (2018) which we denote as “Calib.” We also present the squared kernel calibration error for Gaussian predictions (SKCE) proposed by Widmann et al. (2022). Similarly to Appendix B.4, bold denotes best within first-order methods with the exception of LA-NAM₁₀ where bold means on-par or better.

Table B.7: Calibration error on UCI regression datasets. (Lower is better.)

Model Metric	NAM		LA-NAM		LA-NAM ₁₀	
	Calib. (\downarrow)	SKCE (\downarrow)	Calib. (\downarrow)	SKCE (\downarrow)	Calib. (\downarrow)	SKCE (\downarrow)
autmpg ($n = 392$)	0.054 \pm 0.011	1.9e-3 \pm 7.0e-4	0.037 \pm 0.007	1.8e-3 \pm 3.5e-4	0.043 \pm 0.009	1.5e-3 \pm 4.4e-4
concrete ($n = 1030$)	0.021 \pm 0.007	6.2e-4 \pm 1.6e-4	0.014 \pm 0.004	6.2e-4 \pm 1.3e-4	0.015 \pm 0.005	6.5e-4 \pm 1.2e-4
energy ($n = 768$)	0.042 \pm 0.018	8.3e-3 \pm 4.8e-4	0.040 \pm 0.010	8.9e-3 \pm 4.1e-4	0.042 \pm 0.014	6.1e-3 \pm 1.3e-3
kin8nm ($n = 8192$)	0.015 \pm 0.002	5.6e-5 \pm 1.0e-5	0.012 \pm 0.001	2.7e-6 \pm 4.4e-6	0.007 \pm 0.001	1.4e-5 \pm 4.5e-6
naval ($n = 11934$)	0.176 \pm 0.006	3.1e-8 \pm 4.4e-9	0.077 \pm 0.029	2.7e-9 \pm 1.5e-10	0.026 \pm 0.004	2.2e-9 \pm 1.8e-11
power ($n = 9568$)	0.005 \pm 0.002	2.3e-4 \pm 3.1e-5	0.005 \pm 0.002	1.9e-4 \pm 1.3e-5	0.008 \pm 0.001	1.7e-4 \pm 1.5e-5
protein ($n = 45730$)	0.037 \pm 0.003	1.8e-2 \pm 2.5e-4	0.020 \pm 0.002	1.5e-2 \pm 2.7e-4	0.015 \pm 0.000	1.5e-2 \pm 1.5e-4
wine ($n = 1599$)	0.021 \pm 0.002	1.7e-3 \pm 5.6e-4	0.012 \pm 0.005	6.9e-4 \pm 3.2e-4	0.010 \pm 0.004	5.8e-4 \pm 3.1e-4
yacht ($n = 308$)	0.095 \pm 0.027	1.8e-2 \pm 2.0e-3	0.105 \pm 0.028	1.7e-2 \pm 2.3e-3	0.111 \pm 0.024	1.2e-3 \pm 1.6e-4

Table B.8: Calibration error on UCI classification datasets. (Lower is better.)

Model Metric	NAM		LA-NAM		LA-NAM ₁₀	
	ECE (\downarrow)	RBS (\downarrow)	ECE (\downarrow)	RBS (\downarrow)	ECE (\downarrow)	RBS (\downarrow)
australian ($n = 690$)	0.112 \pm 0.008	0.330 \pm 0.017	0.099 \pm 0.004	0.314 \pm 0.014	0.084 \pm 0.004	0.317 \pm 0.015
breast ($n = 569$)	0.064 \pm 0.018	0.192 \pm 0.013	0.038 \pm 0.005	0.163 \pm 0.010	0.040 \pm 0.004	0.165 \pm 0.009
heart ($n = 270$)	0.153 \pm 0.008	0.356 \pm 0.020	0.136 \pm 0.011	0.314 \pm 0.014	0.150 \pm 0.015	0.315 \pm 0.015
ionosphere ($n = 351$)	0.111 \pm 0.014	0.292 \pm 0.014	0.086 \pm 0.012	0.266 \pm 0.022	0.080 \pm 0.006	0.270 \pm 0.015
parkinsons ($n = 195$)	0.139 \pm 0.006	0.290 \pm 0.019	0.136 \pm 0.009	0.280 \pm 0.023	0.111 \pm 0.006	0.277 \pm 0.025

B.7 Experimental Setup

Linear/Logistic Regression. Implementations are provided by the `scikit-learn` library (Pedregosa et al., 2011). The regularization strength is grid-searched in the set $\{0.001, 0.01, 0.1, 1, 10\}$. For logistic regression, we use the L-BFGS solver performing up to 10,000 iterations.

GAM. We use an open source Python implementation (`pygam`; Servén et al., 2018). The smoothing parameters are grid-searched: We sample one thousand candidates uniformly from the recommended range of $[10^{-3}, 10^3]$ and select using generalized cross-validation scoring (GCV; Golub et al., 1979).

EBM. The explainable boosting machine (EBM) is an open-source Python implementation of the gradient-boosting GAM that is available as a part of the `InterpretML` library (Nori et al., 2019). The library defaults for the hyperparameters performed best. We did not find a significant improvement when tuning the learning rate, maximum number of leaves, or minimum number of samples per leaf.

NAM. We test the NAM with feature networks containing a single hidden layer of 1024 units and ExU activation. We grid-search the learning rate and regularization hyperparameters using the values given in the supplementary material of Agarwal et al. (2021). In practice, we find that combining dropout with a probability of 0.2 and feature dropout of 0.05 along with weight decay of 10^{-5} and a learning rate of either 0.01 or 0.001 gave good results.

LA-NAM. The LA-NAM is constructed using feature networks containing a single hidden layer of 64 neurons with GELU activation (Hendrycks and Gimpel, 2016). Joint feature networks added for second-order interaction fine-tuning contain two hidden layers of 64 neurons. The feature network parameters and hyperparameters (prior precision, observation noise) are optimized using Adam (Kingma and Ba, 2014), alternating between optimizing both at regular intervals, as in Immer et al. (2021a). We select the learning rate in the discrete set of $\{0.1, 0.01, 0.001\}$ which maximizes the ultimate log-marginal likelihood. We use a batch size of 512 and perform early stopping on the log-marginal likelihood restoring the best scoring parameters and hyperparameters at the end of training. We find that the algorithm is fairly robust to the choice of hyperparameter optimization schedule: For all experiments, we use 0.1 for the hyperparameter learning rate and perform batches of 30 gradient steps on the log-marginal likelihood every 100 epochs of regular training.

LightGBM. We use the open-source implementation (Ke et al., 2017). The maximum depth of each tree is selected in the set $\{3, 7, 12\}$, and maximum number of leaves in the set $\{8, 16, 31\}$. Additionally, the minimum number of samples per leaf is reduced to 2 on small datasets from the default of 20. Early stopping is enabled in all experiments, using a 12.5% split of the training data when the task has no predefined validation data. For the HiRID ICU Mortality task in Table 2, we obtain best performance when using the feature engineering recommended in Yèche et al. (2021).

Hardware. The deep learning models are trained on a single NVIDIA RTX2080Ti with a Xeon E5-2630v4 core. Other models are trained on Xeon E5-2697v4 cores and Xeon Gold 6140 cores.

B.8 Illustrative Example

In Section 4.1, we present an illustrative example to motivate the capacity of the LA-NAM and baselines to recover purely additive structure from noisy data. We provide further details on the generation of the synthetic dataset used here. Consider the function $\hat{f} : \mathbb{R}^4 \rightarrow \mathbb{R}$, where $\hat{f}(x_1, x_2, x_3, x_4) = \hat{f}_1(x_1) + \hat{f}_2(x_2) + \hat{f}_3(x_3) + \hat{f}_4(x_4)$, and

$$\hat{f}_1(x_1) = 8(x_1 - \frac{1}{2})^2, \quad \hat{f}_2(x_2) = \frac{1}{10} \exp[-8x_2 + 4] \quad (\text{B.1})$$

$$\hat{f}_3(x_3) = 5 \exp[-2(2x_3 - 1)^2], \quad \hat{f}_4(x_4) = 0. \quad (\text{B.2})$$

We generate $N = 1000$ noisy observations $\{\mathbf{x}_n, y_n\}_{n=1}^N$ by sampling inputs \mathbf{x}_n uniformly from $\mathcal{U}([0, 1]^4)$ and generating targets $y_n = \hat{f}(\mathbf{x}_n) + \epsilon_n$, where $\epsilon_n \sim \mathcal{N}(0, 1)$ is random Gaussian noise. Fig. B.6 shows the recovered functions along with the associated predictive uncertainty for the LA-NAM and baseline models.

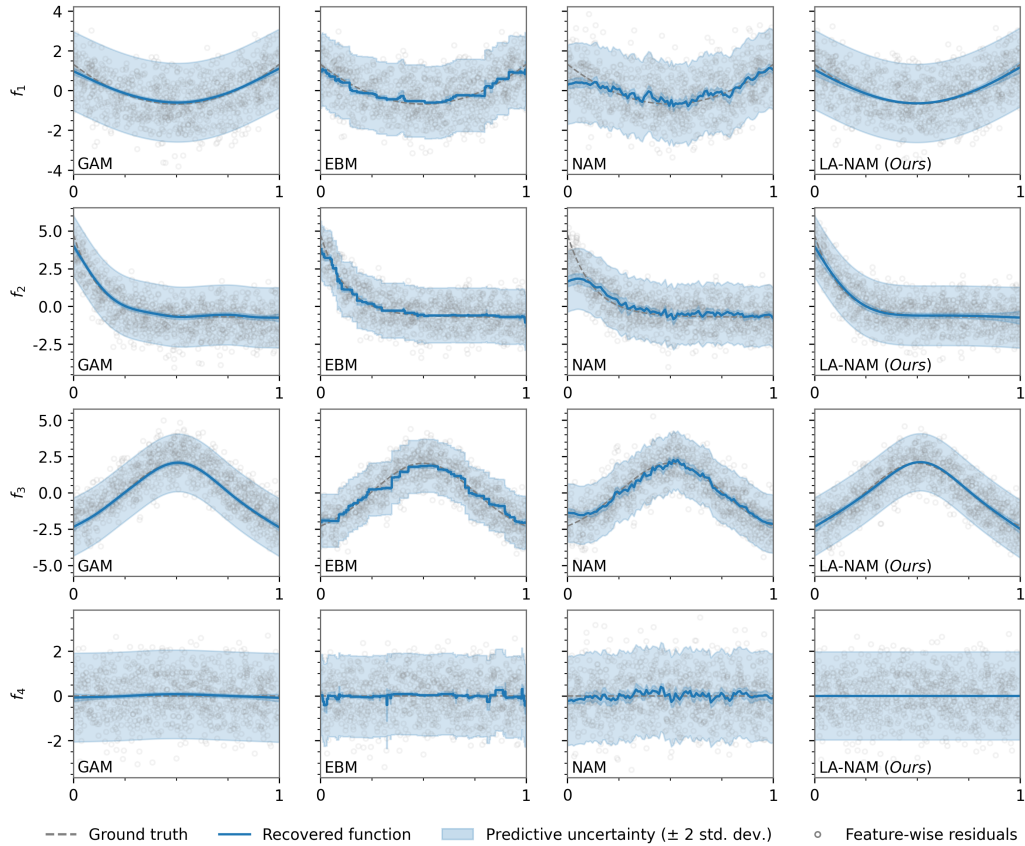


Figure B.6: Recovery of the additive structure of the synthetic dataset of B.8. The feature-wise residuals are the generated data points with mean contribution of the other feature networks subtracted.

B.9 Predicted Mortality Risk in MIMIC-III

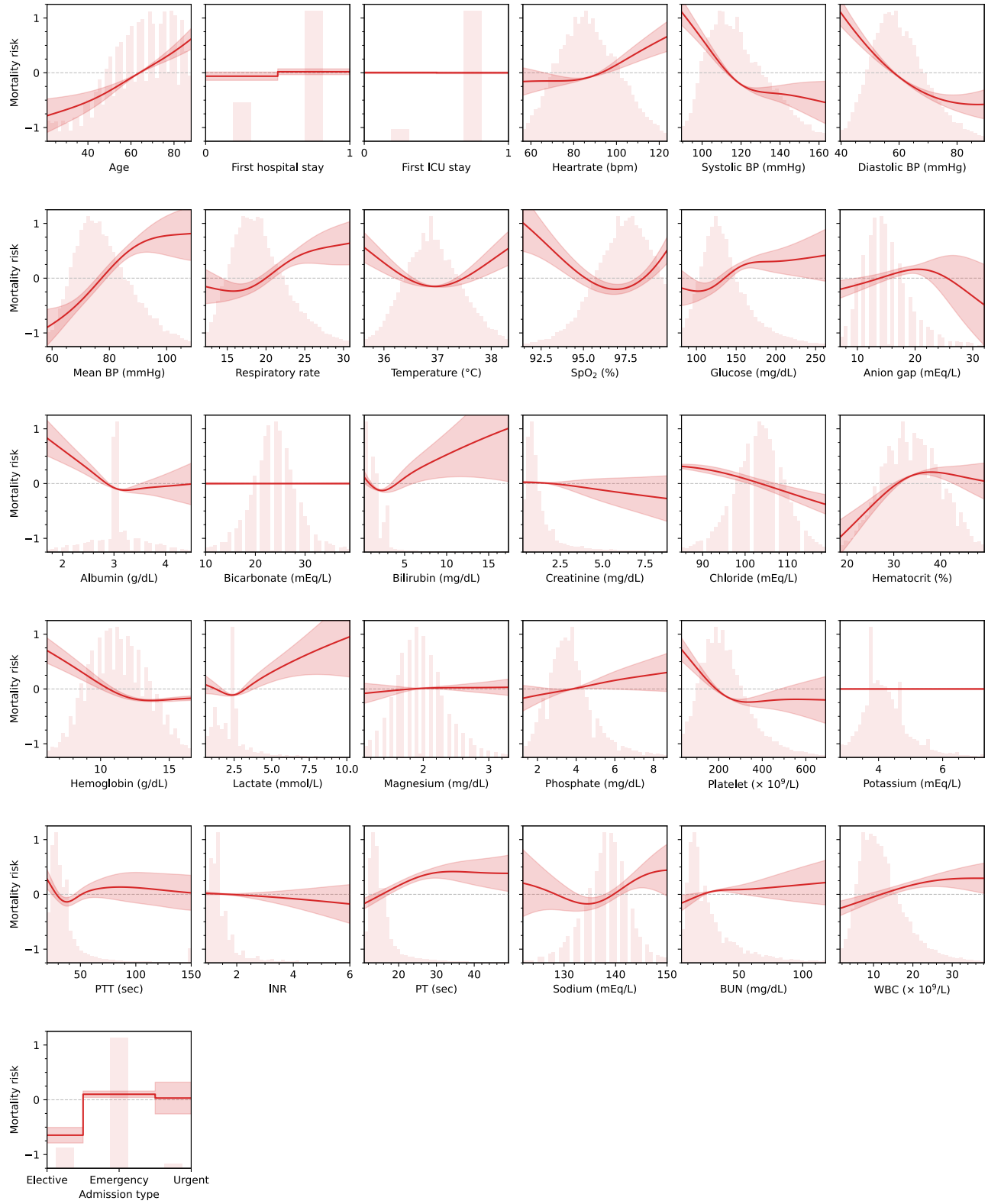


Figure B.7: Complete visualization of the LA-NAM predicted risk in the MIMIC-III mortality task of Section 4.3.

C Detailed Related Work

Generalized additive models. Generalized additive models have been extensively studied and various approaches have been proposed for their construction. Hastie and Tibshirani (1999) initially suggested using smoothing splines (Wahba, 1983) to build the smoothing functions which attend to each feature, fitting them iteratively through “backfitting” (Breiman and Friedman, 1985). One alternative is to construct them using gradient-boosted decision trees (Friedman, 2001). By modifying the boosting algorithm, it becomes possible to cycle through functions in the inner loop, which has been found to be favorable compared to sequential backfitting of boosted trees (Lou et al., 2012). Furthermore, boosted trees facilitate the selection and fitting of feature interactions (Lou et al., 2013). These second-order interactions are believed to contribute to the competitive accuracy achieved by gradient-boosted additive models in comparison to fully interacting models for tabular supervised learning (Caruana et al., 2015; Nori et al., 2019).

Neural additive models. Neural networks are highly attractive for constructing smoothing functions due to their ability to approximate continuous functions with arbitrary precision given sufficient complexity (Cybenko, 1989; Maierov and Pinkus, 1999; Lu et al., 2017). Agarwal et al. (2021) proposed the neural additive model (NAM), which utilizes ensembles of feed-forward networks and employs standard backpropagation for fitting. To accommodate jagged functions, they introduced “ExU” dense layers, wherein weights are learned in logarithmic space.

A closely related model, called GAMI-Net, was introduced by Yang et al. (2021), but it employs single networks instead of an ensemble and additionally supports the learning of feature interaction terms. In the GAMI-Net, the feature pair candidates are selected for feature interaction fine-tuning using the ranking procedure of Lou et al. (2013). Yang et al. (2021) acknowledge that this ranking can also be done using neural networks with the approach proposed by Tsang et al. (2018). Alternatively, one can avoid having to select pairs entirely by finding a scalable formulation for all possible pairs, such as in the neural basis model (NBM) of Radenovic et al. (2022). In this work, we propose to rank the feature pair candidates using the available posterior approximation.

Many other extensions have been suggested, including feature selection through sparse regularization of the feature networks (Xu et al., 2022), generation of confidence intervals using regression spline basis expansion (Luber et al., 2023), and estimation of the skewness, heteroscedasticity, and kurtosis of the underlying data distributions (Thielmann et al., 2023).

Bayesian neural networks. Bayesian neural networks offer the potential to combine the expressive capabilities of neural networks with the rigorous statistical properties of Bayesian inference (MacKay, 1992; Neal, 1993). However, achieving accurate inference in these complex models has proven to be a challenging endeavor (Jospin et al., 2022). The field has explored various techniques for approximate inference, each with its own trade-offs in terms of quality and computational cost.

At one end of the spectrum, we have inexpensive local approximations such as Laplace inference (Laplace, 1774; MacKay, 1992; Khan et al., 2019; Daxberger et al., 2021a) which provides a simple and computationally efficient solution. Other approaches in this category include stochastic weight averaging (Izmailov et al., 2018; Maddox et al., 2019) and dropout (Gal and Ghahramani, 2016; Kingma et al., 2015).

Moving towards more sophisticated approximations, variational methods come into play, offering a range of complexity levels. Researchers have proposed diverse variational approximations, including work by Graves (2011); Blundell et al. (2015); Louizos and Welling (2016); Khan et al. (2018); Osawa et al. (2019). Ensemble-based methods have also been explored as an alternative avenue. This includes recent work by Lakshminarayanan et al. (2017); Wang et al. (2019); Wilson and Izmailov (2020); Ciosek et al. (2020); He et al. (2020); D’Angelo et al. (2021); D’Angelo and Fortuin (2021).

On the other end of the spectrum, we find Markov Chain Monte Carlo (MCMC) approaches, which provide asymptotically correct solutions. Neal (1993); Neal et al. (2011); Welling and Teh (2011); Garriga-Alonso and Fortuin (2021); Izmailov et al. (2021) have contributed to the exploration of these computationally expensive yet theoretically accurate methods.

Beyond the challenges related to approximate inference, recent work has also studied the question of prior choice for Bayesian neural networks (e.g., Fortuin et al., 2021, 2022; Fortuin, 2022; Nabarro et al., 2022; Sharma et al.,

2023, and references therein). Additionally, model selection within the Bayesian neural network framework has garnered attention (e.g., Immer et al., 2021a, 2022b,a; Rothfuss et al., 2021, 2022; van der Ouderaa and van der Wilk, 2022; Schwöbel et al., 2022).

In our work, we focus primarily on leveraging the linearized Laplace inference technique proposed by Immer et al. (2021b). We also utilize the associated marginal likelihood estimation method introduced by Immer et al. (2021a). These methods, to the best of our knowledge, have not been previously applied to the NAM.